Perovskite phase formation and ferroelectric properties of the lead nickel niobate–lead zinc niobate–lead zirconate titanate ternary system

Naratip Vittayakorn, Gobwute Rujijanagul, and Tawee Tunkasiri
Department of Physics, Faculty of Science, Chiang Mai University, Chiang Mai 50200 Thailand

Xiaoli Tan and David P. Cann
Materials Science and Engineering Department, Iowa State University, Ames, Iowa 50011

The ternary system of lead nickel niobate $Pb(Ni_{1/3}Nb_{2/3})O_3$ (PNN), lead zinc niobate $Pb(Zn_{1/3}Nb_{2/3})O_3$ (PZN), and lead zirconate titanate $Pb(Zr_{1/2}Ti_{1/2})O_3$ (PZT) was investigated to determine the influence of different solid state processing conditions on dielectric and ferroelectric properties. The ceramic materials were characterized using x-ray diffraction, dielectric measurements, and hysteresis measurements. To stabilize the perovskite phase, the columbite route was utilized with a double crucible technique and excess PbO. The phase-pure perovskite phase of PNN–PZN–PZT ceramics was obtained over a wide compositional range. It was observed that for the ternary system $0.5PNN–(0.5 − x)PZN–xPZT$, the change in the transition temperature (T_m) is approximately linear with respect to the PZT content in the range $x = 0$ to 0.5. With an increase in x, T_m shifts up to high temperatures. Examination of the remanent polarization (P_r) revealed a significant increase with increasing x. In addition, the relative permittivity (ϵ_r) increased as a function of x. The highest permittivities ($\epsilon_r = 22,000$) and the highest remanent polarization ($P_r = 25 \ \mu C/cm^2$) were recorded for the binary composition $0.5Pb(Ni_{1/3}Nb_{2/3})O_3–0.5Pb(Zr_{1/2}Ti_{1/2})O_3$.

I. INTRODUCTION

Lead-based complex perovskites, such as $Pb(Zn_{1/3}Nb_{2/3})O_3$ (PZN) and $Pb(Ni_{1/3}Nb_{2/3})O_3$ (PNN), having the general formula $Pb(B'B'')O_3$ have received significant attention since the 1970s because of their peculiar dielectric and piezoelectric behavior. These materials have been applied in many areas such as electrostrictive actuators, transducers, and multilayer ceramic capacitors.[1–6]

Lead zinc niobate, PZN, was first synthesized in the 1960s.[7] Its permittivity versus temperature curve displayed a broad peak around 140 °C (T_m) with a strong frequency dependence. Extremely high relative permittivities have been measured in the vicinity of the peak with a $\epsilon_r \sim 60,000$ reported for single crystals.[4,8–11] Nanometer-level chemical heterogeneity in the form of short range order of Zn^{2+} and Nb^{5+} at B-sites was proposed to account for the observed diffuse phase transition.[12,13] The crystal structure of PZN is rhombohedral ($3m$) at room temperature and transforms to cubic ($Pm3m$) at high temperatures.

Unfortunately, phase-pure perovskite PZN polycrystalline ceramics have not been synthesized by conventional solid-reaction methods because of a steric and an electrostatic interaction between high polarization of the Pb^{2+} cation and the Zn^{2+} cation, which favors the formation of the pyrochlore phase instead of the perovskite phase.[14] Moreover, the low tolerance factor and small electronegativity difference[2] makes the perovskite phase unstable, requiring the addition of normal ferroelectric compounds such as $BaTiO_3$[15] and $PbTiO_3$[16] to stabilize the perovskite phase. Recently, Fan et al.[17,18] mixed $Pb(Zr_{0.47}Ti_{0.53})O_3$ with PZN by a conventional solid-state reaction method and successfully stabilized perovskite PZN. A morphotropic phase boundary (MPB) between the PZN-rich rhombohedral phase and the PZT-rich tetragonal phase was reported at PZN:PZT47/53 $= 1:1$. At this composition, a high electromechanical coupling factor of $k_p = 0.67$ was measured.

Lead nickel niobate (PNN) exhibits a diffuse phase transition around −120 °C with a much lower peak permittivity of about 4000.[19] The crystal structure of PNN at room temperature is cubic ($Pm3m$) with a lattice parameter of 4.03 Å.[19] Phase-pure perovskite PNN can be prepared via the columbite method.[2,20] Luff et al.[21] investigated solid solutions in the PNN–$PbTiO_3$–$PbZrO_3$ system and identified the composition of 0.5PNN–0.35PT–0.15PZ with optimal piezoelectric properties. Detailed reaction kinetics during solid state processing of

PNN–PZT was recently investigated by Babushkin and several pyrochlore phases have been detected.[22] The piezoelectric PNN–PZT ceramics have found wide applications and are now commercially available.

The investigation of the ferroelectric properties of the PNN–PZN–PZT ternary system is of interest for a number of reasons. Both PNN and PZN have distinct transition temperatures, and the transition temperature for the solid solution of PNN–PZN should lie in the ambient temperature range. This implies that the ultrahigh permittivity values can be realized at room temperature. As demonstrated in the binary PZN–PZT and PNN–PZT systems, the addition of PZT imparts superior piezoelectric properties to the solid solutions. Therefore, there is great potential for excellent dielectric and piezoelectric properties within the ternary system PNN–PZN–PZT.

Information in the literature on the PNN–PZN–PZT ternary system is extremely limited. Lee *et al.*[23] tried to fabricate phase-pure perovskite PNN–PZN–PZT ceramics with a Zr/Ti ratio in PZT of 1.0. In their study, powders of PZT, PZN, and PNN were prepared separately and then mixed and calcined again to form perovskite PNN–PZN–PZT. The highest amount of perovskite phase in their work was found to be 92%. The Curie temperature was found to vary from 50 to 250 °C, depending on the mol fraction of PZT. The best piezoelectric properties at room temperature, $k_p = 0.63$, were found in the composition 0.5PNN–0.3PZN–0.2PZT.

The presence of pyrochlore phase is extremely detrimental to the dielectric and piezoelectric properties in most perovskite ceramics. The process of prereacting the B-site cations to form a columbite phase $B'B''_2O_6$ prior to the addition of PbO has been successfully applied to many systems to suppress pyrochlore phase formation.[2,20,24,25] However, this technique has been largely unsuccessful for PZN and fabrication of phase-pure PZN-containing solid solutions remains a challenging issue. In this work, a processing route different from that used previously by Lee *et al.*[23] was used to successfully prepare phase-pure perovskite PNN–PZN–PZT ceramics. The use of the double crucible technique, using excess PbO, and maintaining a fast heating rate were all found to be essential factors in perovskite phase development. Dielectric and ferroelectric properties of single-phase perovskite ceramics are reported in the present article and piezoelectric characterization is underway and will be published in a separate paper.

II. EXPERIMENTAL

In this method, the columbite precursors $ZnNb_2O_6$ and $NiNb_2O_6$ were prepared from the reaction between ZnO (99.9%) and Nb_2O_5 (99.9%) at 975 °C for 4 h and between NiO (99.9%) and Nb_2O_5 (99.9%) for 4 h at 1100 °C, respectively.[24,25] The wolframite phase $ZrTiO_4$ was formed by reacting ZrO_2 (99.9%) with TiO_2 (99.9%) at 1400 °C for 4 h.[26] The powders of $ZnNb_2O_6$, $NiNb_2O_6$, and $ZrTiO_4$ were mixed in the required stoichiometric amounts with PbO (99.9%) with an excess of 2 mol% of PbO added. The compositions synthesized in this study were $x = 0$, 0.1, 0.3, and 0.5 in the ternary system $0.5PNN–(0.5 − x)PZN–xPZT$. The milling process was carried out for 24 h in isopropyl alcohol. After drying at 120 °C, the powders were calcined at 900–950 °C for 4 h in a double crucible configuration with a heating rate of 20 °C/min. After grinding and sieving, 5 wt.% of polyvinyl alcohol binder was added. Disks with a diameter of 1.5 cm were prepared by cold uniaxial pressing at a pressure of 150 MPa. Binder burnout occurred by slow heating to 500 °C and holding for 2 h. To investigate the sintering behavior, the disks were sintered in a sealed alumina crucible at temperatures ranging from 950 to 1250 °C using a heating rate of 5 °C/min and a dwell time of 2 h. To prevent PbO volatilization from the disks, a PbO atmosphere was maintained by placing $PbZrO_3$ powders in the crucible. Phase formation and crystal structure of the calcined powders and sintered discs were examined by x-ray diffraction (XRD). Data collection was performed in the 2θ range of 20–60° using step scanning with a step size of 0.02° and counting time of 2 s/step. The relative amounts of perovskite and pyrochlore phase were determined by measuring the primary x-ray peak intensities of the perovskite and pyrochlore phase. The percentage of perovskite phase was estimated by the following equation:

$$\% \text{ perovskite phase} = \left(\frac{I_{\text{perov}}}{I_{\text{perov}} + I_{\text{pyro}} + I_{\text{PbO}}} \right) \times 100 \quad ,$$

(1)

where I_{perov}, I_{pyro}, and I_{PbO} refer to the intensity of the (110) perovskite peak, and the intensity of the (220) pyrochlore and PbO peaks, respectively. The pellets were polished and electroded via gold sputtering, over which a layer of air-dried silver paint was applied. The relative permittivity (ϵ_r) and dissipation factor (tan δ) of the pellets sample were measured at various temperatures ranging from −100 to 180 °C with a heating and cooling rate of 3 °C/min over the frequency range between 100 Hz and 100 kHz using an LCR meter (HP 4284A, Tokyo, Japan) in conjunction with a Delta Design 9023 (San Diego, CA) temperature chamber. The remanent polarization P_r was determined from a P-E hysteresis loop measurements using a Sawyer–Tower circuit at temperatures between −66 and 60 °C.

III. RESULTS AND DISCUSSION

A. Perovskite phase development

The perovskite and pyrochlore phase formation at different calcination temperatures in $0.5PNN–(0.5 − x)PZN–xPZT$ powders with $x = 0.1$ to 0.5 were studied

J. Mater. Res., Vol. 18, No. 12, Dec 2003

2883

and analyzed by XRD. XRD patterns from this system are given in Fig. 1. The cubic pyrochlore-type structure of $Pb_{1.83}(Nb_{1.71}Zn_{0.29})O_{6.39}$[27] was identified in the x = 0.0, 0.1, and 0.3 compositions at the 900 °C calcination temperature. The pyrochlore formation reaction from PbO and the columbite precursors is an extremely fast process, which is completed within 2–3 min at temperatures as low as 750 °C.[28] With increased calcination temperatures the amount of perovskite phase increased sharply. In our work, it was observed that the primary phase in all of the compositions at 950 °C was well-crystallized perovskite. Within the detection limits of the XRD technique, the samples were essentially 100% perovskite and free of pyrochlore. The heat treatment and percent perovskite phase for all the compositions are listed in Table I. The first two rows listed are for the calcined powders, and the remaining data are derived from sintered samples using powders calcined at 950 °C.

In this study, the combination of using a double crucible, excess PbO (2 mol%), and a fast heating/cooling rate (20 °C/min) were shown to be effective in reducing the total amount of pyrochlore phase during calcination at 950 °C. The 2 mol% excess PbO was chosen

because there were observations reported that compositions with excess PbO additions greater than 2.8 mol% resulted in degraded electrical properties. This was attributed to the presence of an excess PbO layer at the grain boundary.[29,30]

XRD patterns from a set of samples prepared at various sintering temperatures are given in Fig. 2. In this study, for the x = 0 composition single-phase perovskite was obtained for sintering temperatures below 1150 °C. Above 1150 °C, the cubic pyrochlore phase $Pb_{1.83}(Nb_{1.71}Zn_{0.29})O_{6.39}$[27] formed and the percentage of pyrochlore phase increased as the sintering temperature increased, as shown in Table I. This behavior also appeared in the x = 0.1 composition at sintering temperatures above 1200 °C. The behavior is believed to be due to the volatilization of PbO at high temperatures. Nevertheless, the XRD patterns for the x = 0.3 and 0.5 compositions do not show the formation of the

TABLE I. Perovskite phase development during calcinations and sintering process of $0.5PNN–(0.5 − x)PZN–xPZT$ system. (The first two rows indicate the data in calcined powders and the rest of the rows are data from sintering of powders calcined at 950 °C.)

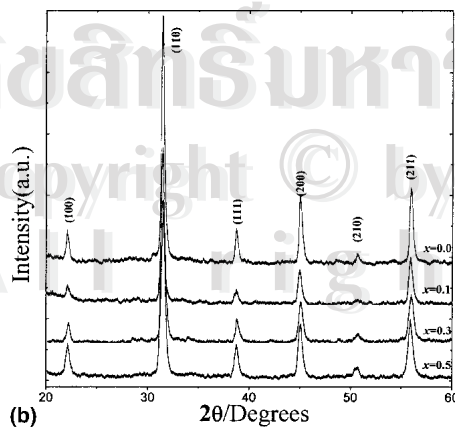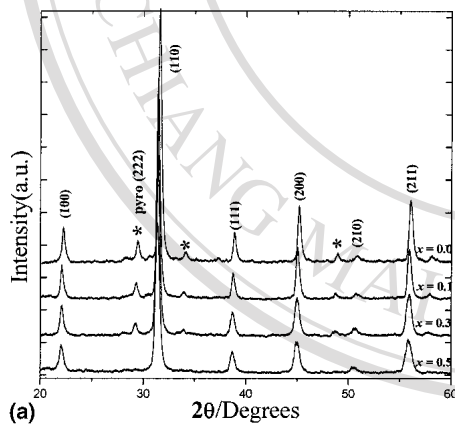| Temperature (°C)	Perovskite phase (%)			
	x = 0.0	x = 0.1	x = 0.3	x = 0.5
900[a]	91.53	92.67	92.5	100
950[a]	100	100	100	100
1000	100	100	⋯	⋯
1050	100	100	100	⋯
1100	100	100	100	⋯
1150	100	100	100	100
1200	84.468	100	100	100
1225	76.249	76.79	100	100
1250	⋯	⋯	100	100
1275	⋯	⋯	100	100

[a]Calcination temperatures.

FIG. 1. Powder XRD patterns of a stoichiometric composition of $0.5PNN–(0.5 − x)PZN–xPZT$ ceramics: (a) calcined at 900 °C for 4 h with 20 °C/min heating rate, (b) calcined at 950 °C for 2 h with 20 °C/min heating rate; pyrochlore phase indicated with (*).
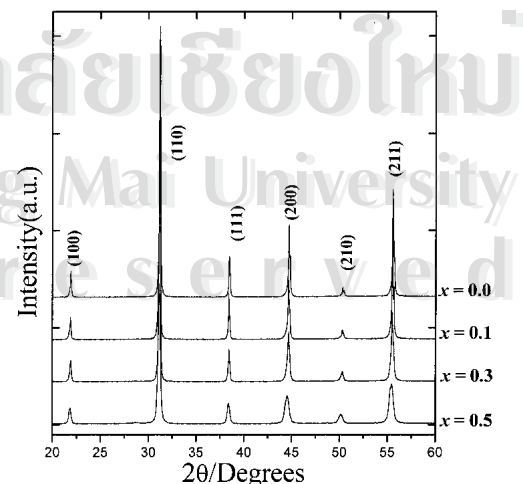

FIG. 2. XRD patterns of $0.5PNN–(0.5 − x)PZN–xPZT$ ceramics at the optimum sintering conditions.

pyrochlore phase. It is interesting to note that the intensity of (100) perovskite peak decreased at high temperatures for the $0.1 \leq x \leq 0.5$ composition.

In the PNN–PZN–PZT system, the A-site is occupied by Pb^{2+} (1.630 Å) ions, and the Ni^{2+}, Nb^{5+}, Zn^{2+}, Zr^{4+}, and Ti^{4+} ions occupy the B site of the ABO_3 perovskite crystal structure. The average ionic radius of B-site ions in the composition $0.5Pb(Ni_{1/3}Nb_{2/3})O_3$–$(0.5 - x)$$Pb(Zn_{1/3}Nb_{2/3})O_3$–$xPb(Zr_{1/2}Ti_{1/2})O_3$ can be calculated from the following equation:

$$r_{B-site} = 0.5 \left\lfloor \tfrac{1}{3}r_{Ni^{2+}} + \tfrac{2}{3}r_{Nb^{5+}} \right\rfloor + (0.5 - x) \left\lfloor \tfrac{1}{3}r_{Zn^{2+}} + \tfrac{2}{3}r_{Nb^{5+}} \right\rfloor + x \left\lfloor \tfrac{1}{2}r_{Zr^{4+}} + \tfrac{1}{2}r_{Ti^{4+}} \right\rfloor , \quad (2)$$

where the ionic radii of Ni^{2+}, Nb^{5+}, Zn^{2+}, Zr^{4+}, and Ti^{4+} are 0.830, 0.780, 0.880, 0.860 and 0.745 Å, respectively.[31] A simple description of the geometric packing within perovskite structure can be characterized by tolerance factor t, which is defined by the following equation:[5,8,13,32]

$$t = \frac{(r_A + r_O)}{\sqrt{2}(r_B + r_O)} , \quad (3)$$

where r_A, r_B, and r_O are the ionic radii of the A, B and O ions, respectively. The calculated average B-site ionic radii and tolerance factor of the PNN–PZN–PZT system is presented in Table II using 1.260 Å for the radius of O^{2-}.[31] The effective size of the B-site ion decreases with an increasing mol faction of PZT primarily due to the smaller ionic radii of Ti^{4+}. This results in a slight increase in the tolerance factor as it approaches 1.0. However, the lattice parameter is found to increase as the mol faction of PZT increases, and the symmetry changes from pseudocubic to rhombohedral.

The crystal symmetry of PNN at room temperature was determined to be pseudo-cubic perovskite with a cell parameter $a = 4.0308$ Å. The PZN composition at room temperature was determined to be the rhombohedral space group $R3m$. According to the $PbZrO_3$–$PbTiO_3$ phase diagram, at room temperature $Pb(Zr_{1/2}Ti_{1/2})O_3$ is within the tetragonal phase field near the MPB region.[33] In this work, the crystal structure and lattice parameters of the PNN–PZN–PZT compositions were determined through room temperature diffraction experiments. The indexing procedure of the perovskite phase in the

$x = 0.0$ and $x = 0.1$ samples was performed based on cubic symmetry. For the $x = 0.3$ and 0.5 samples, however, no splitting of 002 and 200 peak was observed with increased PZT concentration, as shown in Fig. 2. However, the superposition was clearly observed for the (220) peak as shown in Fig. 3. This result indicates that the crystal structure was rhombohedral. In addition, from the data listed in Table II, it is evident that the lattice parameter a increased with increasing concentration of PZT due to the increase in B-site radius.

B. Dielectric properties

The permittivity at 1 kHz as a function of temperature for $0.5PNN$–$(0.5 - x)PZN$–$xPZT$ ceramics under different sintering conditions is shown in Fig. 4. The sintering temperature was found to have a significant effect on the
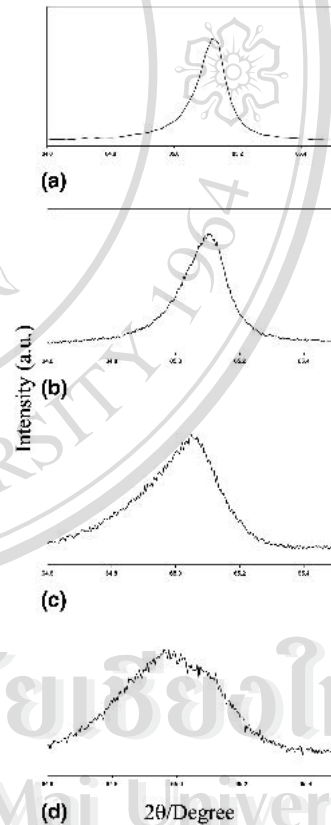

FIG. 3. XRD patterns of the (220) peak of $0.5PNN$–$(0.5 - x)PZN$–$xPZT$ ceramics: (a) $x = 0$, (b) $x = 0.1$, (c) $x = 0.3$, (d) $x = 0.5$.

TABLE II. Comparison of the calculated average B-site ionic radii, the crystal structure, and lattice parameters derived from XRD data.

Composition $0.5PNN$–$(0.5 - x)PZN$–$xPZT$	Average B-site ionic radii (Å)	Tolerance factor, t	Lattice parameter, a (Å)	Crystal structure	Distortion angle, α
$x = 0.0$	0.8050	0.9896	4.049	Cubic	90.0
$x = 0.1$	0.8039	0.9901	4.054	Cubic	90.0
$x = 0.3$	0.8018	0.9912	4.057	Rhombohedral	89.88
$x = 0.5$	0.7996	0.9922	4.060	Rhombohedral	89.89

permittivity. All compositions exhibited an increase in the permittivity with increased sintering temperatures. However, at the highest sintering temperature the permittivity decreased due to the formation of a pyrochlore phase. The $x = 0$ composition showed an increase in permittivity up to a maximum of 10,000 at a sintering temperature of 1150 °C. At higher sintering temperatures there is both a decrease in permittivity and a shift in the temperature at which the permittivity is maximum (T_m)

from −20 to −50 °C. This shift in T_m is likely to be the result of a change in the stoichiometry of the perovskite phase due to the effects of Zn volatilization and the formation of the pyrochlore phase $Pb_{1.83}(Nb_{1.71}Zn_{0.29})O_{6.39}$. This shifted the overall perovskite composition closer to PNN, with a lower T_m of −120 °C. In addition, the decrease in permittivity that was observed was the result of the low permittivity of $Pb_{1.83}(Nb_{1.71}Zn_{0.29})O_{6.39}$ ($\epsilon_r \sim 100$).
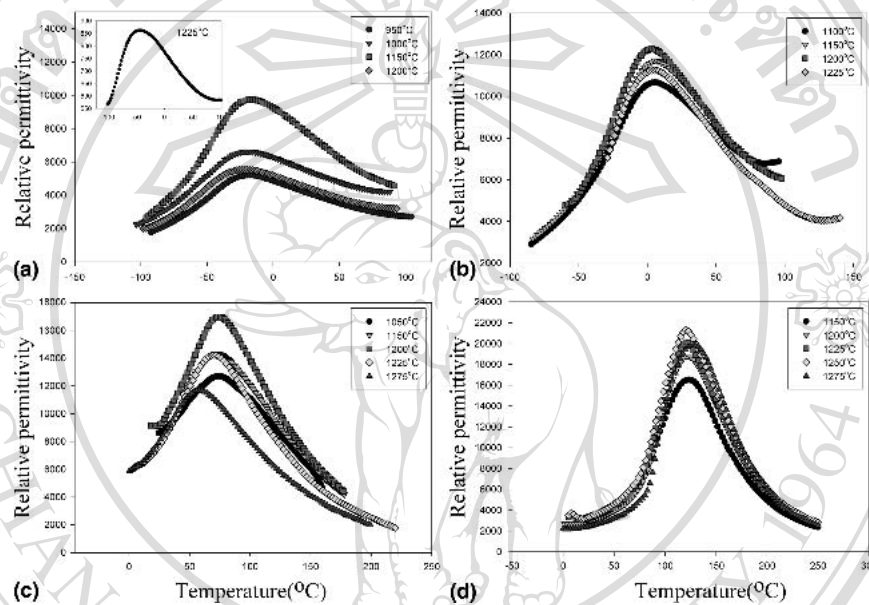

FIG. 4. Relative permittivity and dissipation factor at 1kHz for 0.5PNN–(0.5 − x)PZN –xPZT: (a) $x = 0$, (b) $x = 0.1$, (c) $x = 0.3$, (d) $x = 0.5$. Dielectric data for different sintering temperatures is shown.
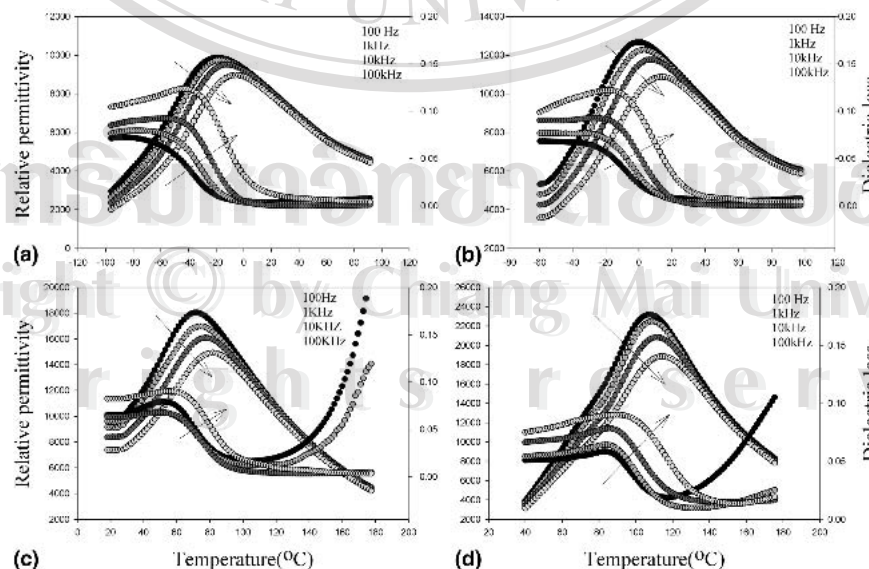

FIG. 5. Relative permittivity and dissipation factor of 0.5PNN–(0.5 − x)PZN–xPZT ceramics prepared at the optimum sintering conditions. (a) $x = 0$, ceramics sintered at 1150 °C for 2 h; (b) $x = 0.1$, ceramics sintered at 1200 °C for 2 h; (c) $x = 0.3$, ceramics sintered at 1200 °C for 2 h; (d) $x = 0.5$, ceramics sintered at 1250 °C for 2 h.

The $x = 0.1$ composition exhibited a maximum permittivity of approximately 12,000 with a $T_m \sim 0\ °C$ at a sintering temperature of 1200 °C. Higher sintering temperatures resulted in a decrease in the permittivity. Likewise the $x = 0.3$ composition exhibited a maximum permittivity of 17,000 at $T_m = 70\ °C$ at a sintering temperature of 1200 °C. Consistent with the other compositions, increased sintering temperatures resulted in a decrease in permittivity and a shift in T_m. Finally, the highest permittivities in this study were recorded for the $x = 0.5$ composition at a sintering temperature of 1250 °C with $\epsilon_{r,max} = 22,000$ at $T_m \sim 120\ °C$. This is significantly larger than the previous value reported in the literature.[23]

In this work, the dielectric experiments showed that the optimum sintering conditions for $0.5PNN–(0.5 − x)$ $PZN–xPZT$ were for 2 h at 1150, 1200, 1200, and 1250 °C, for the $x = 0$, $x = 0.1$, $x = 0.3$, and $x = 0.5$ compositions, respectively. Ceramics sintered under these conditions were used in the determination of the crystal structure and lattice parameters, which had been shown in Figs. 2 and 3, and Table II. The following

characterization of the dielectric and ferroelectric properties of each composition was also carried out in sample sintered at their optimum conditions.

Figure 5 shows the dielectric properties for each composition at the optimum sintering conditions. All of compositions showed a broadening of the permittivity maxima and the T_m increased with increasing measurement frequency, as expected. Experimental results indicate that all of compositions show a diffuse phase transition with the strong frequency dispersion, which is characteristic of relaxor ferroelectrics.[1,3,12,34] From this result, it is clear from the sharpness of the permittivity peak that the compositions gradually approached normal ferroelectric behavior as the mol fraction of PZT increased. As x approached 0, the behavior was strongly relaxor in nature. This may be a function of the degree of B-site cation ordering or the influence of the macro-domains.

In general, the sintering temperature of this system increased with increased mol percent of PZT. Both the maximum permittivity, $\epsilon_{r,max}$ and T_m increased quasi-linearly as the molar fraction of PZT increased. The T_m of the constituent compounds PNN, PZN, and PZT are −120, 140, and 390 °C, respectively,[10,19,33] which can be used to calculate an empirical estimate of T_m via the equation:

$$T_m = 0.5 \times (−120\ °C) + (0.5 − x) \times (140\ °C) + x \times (390\ °C) \ . \tag{4}$$

The variation of the measured T_m, the calculated T_m, and the measured $\epsilon_{r,max}$ with composition x is shown in Fig. 6. It is evident that Eq. (4) gives a reasonable indication of the transition temperature T_m. A summary of the dielectric properties for each of the compositions is shown in Table III. As Table III illustrates, the PNN–PZN–PZT ceramics in this study resulted in significantly higher permittivities than in previous studies. Through controlling PbO loss and preventing pyrochlore phase formation, single-phase perovskite ceramics can be processed with excellent electrical properties.

FIG. 6. T_m, calculated T_m, and maximum relative permittivity as a function of composition x at 1 kHz.

TABLE III. Comparisons of dielectric properties of ceramics in the $0.5PNN–(0.5 − x)$ $PZN–xPZT$ system at the optimum sintering conditions.

	Composition $0.5PNN–(0.5 − x)PZN–xPZT$	Percent perovskite	T_m (°C)	Relative permittivity (at 25 °C) at 1 kHz	Relative permittivity (at T_m) at 1 kHz	Dielectric loss (at 25 °C) at 1 kHz
Lee *et al.*[23]	$x = 0.0$	85	55	4000	6000	⋯
	$x = 0.1$	87	80	4700	8000	⋯
	$x = 0.3$	92	140	5500	13000	⋯
	$x = 0.5$	78	225	2500	7000	⋯
Vierheilig *et al.*[37]	$x = 0.0$	100	−10	6077	6980	0.010
This work	$x = 0.0$	100	−20	8500	9700	0.011
	$x = 0.1$	100	0	11500	13000	0.032
	$x = 0.3$	100	70	9000	18000	0.050
	$x = 0.5$	100	125	4000	22000	0.048

C. Ferroelectric properties

Polarization hysteresis measurements at room temperature were performed using a modified Sawyer–Tower circuit. The hysteresis loops as a function of x are shown in Fig 7. The $x = 0$ and $x = 0.1$ compositions exhibited slim loops characteristic of relaxor ferroelectrics. The saturation polarization P_s, remanent polarization P_r, and coercive field E_c were increased with increased mol percent of PZT as illustrated in Table IV. The loop area values were calculated by integrating the polarization with respect to the electric field. The maximum remanent polarization was observed for the $x = 0.5$ composition. The values of P_s, P_r, and E_c for the $x = 0.5$ composition are 31.9 μC/cm^2, 25.2 μC/cm^2, and 4.0 kV/cm, respectively.

These hysteresis data are consistent with the dielectric results in illustrating the gradual trend from relaxor to normal ferroelectric as the mol fraction of PZT is increased.[1,35,36] The hysteresis loops for the compositions $x = 0$ and $x = 0.3$ at various temperatures are shown in Fig. 8. The coercive field values for each composition

were found to exhibit an increase with decreased temperature. This is due to the influence of the metastable macro-domain structure and the immobilizations of the domain walls.[1,35,36]

The $x = 0.3$ and 0.5 compositions exhibited square loop behavior at −66 °C. However, as the temperature increased the square loops transformed to slim loops and the remanent polarization and coercive filed values decreased significantly. The $x = 0$ and $x = 0.1$ compositions exhibited slim loop behavior near room temperature. All of compositions displayed a clear transition from square-loop behavior to slim-loop behavior in

TABLE IV. Polarization hysteresis data as a function of x in the 0.5PNN–(0.5 − x)PZN–xPZT system.

Composition	P_s (μC/cm^2)	P_r (μC/cm^2)	E_c (kV/cm)	Loop area (mC/cm^3)
$x = 0.0$	22.5	0.9	0.008	49.88
$x = 0.1$	23.8	1.8	0.010	72.81
$x = 0.3$	28.1	8.5	1.221	255.12
$x = 0.5$	31.9	25.2	4.024	628.47

$x = 0.0$

$x = 0.1$

$x = 0.3$

$x = 0.5$
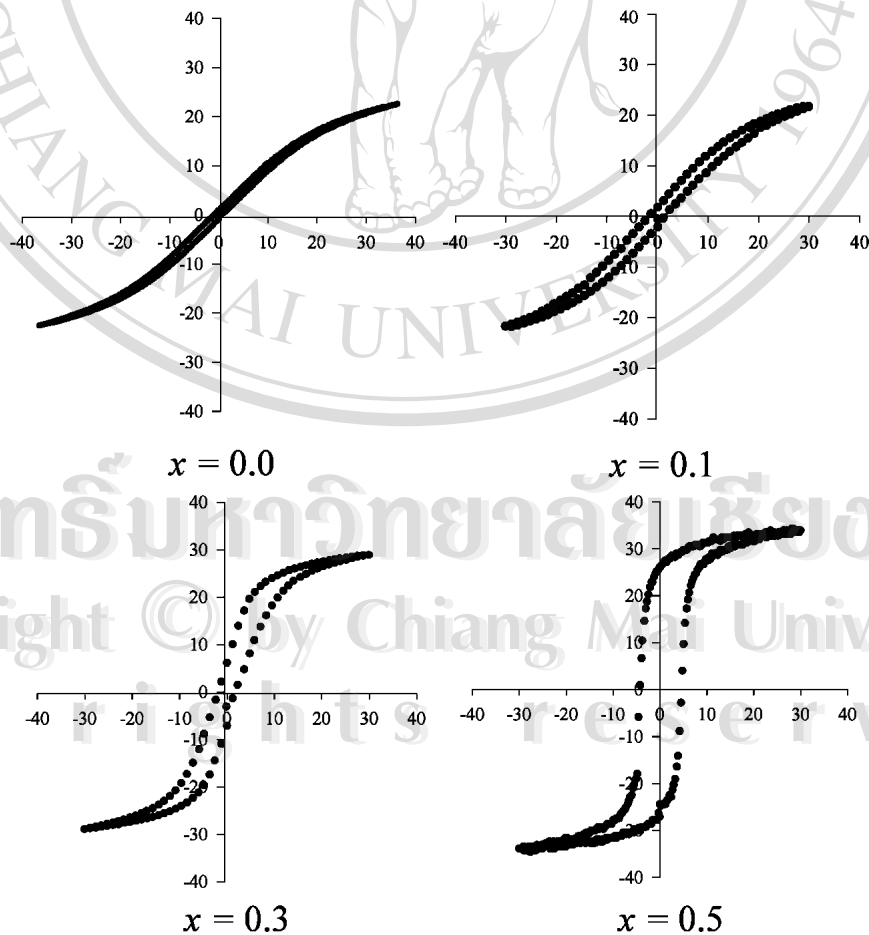
FIG. 7. Room-temperature polarization versus electric field hysteresis loops for 0.5PNN–(0.5 − x)PZN–xPZT ceramics at the optimum sintering conditions.
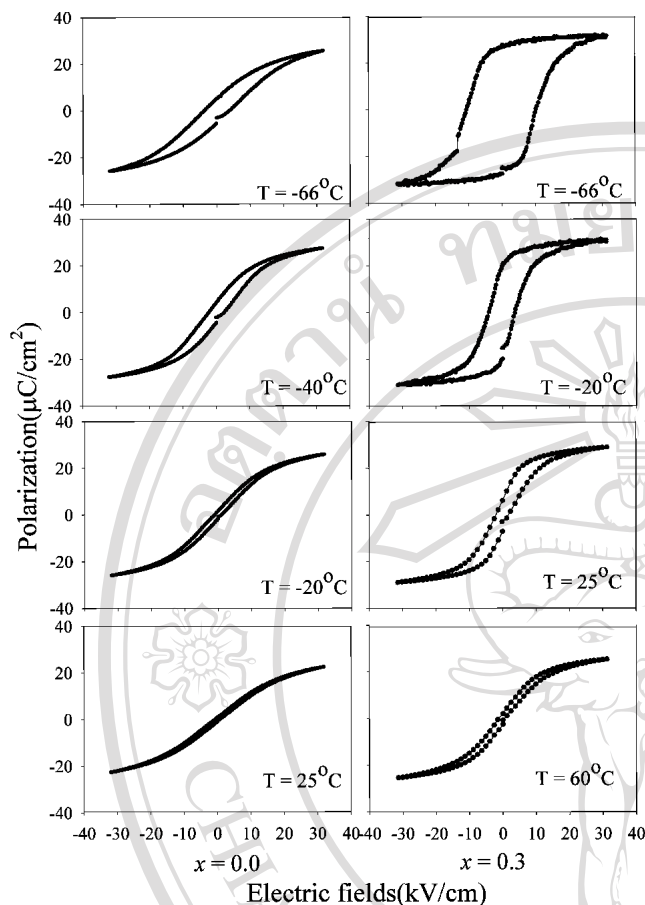
FIG. 8. Temperature dependence of the *P–E* hysteresis of 0.5PNN–$(0.5 - x)$PZN–xPZT ceramics at optimum sintering conditions, compositions $x = 0$ and $x = 0.3$ are shown

the vicinity of T_m. In addition, the hysteresis loops showed that the remanent polarization is nonzero at T_m but decays to zero at temperatures above T_m.

IV. CONCLUSIONS

In this work, it was shown that by controlling PbO loss and preventing pyrochlore formation high permittivity ceramics in the PNN–PZN–PZT system can be processed through high-temperature calcination. This can be accomplished by utilizing a double crucible during calcination, adding excess PbO (2mol%), and maintaining a fast heating/cooling rate (20 °C/min). The dielectric properties and the T_m of 0.5PNN–$(0.5 - x)$PZN–xPZT was found to increase with increasing PZT concentration. Furthermore, the transition from the normal ferroelectric to the relaxor ferroelectric state was clearly observed as the mol fraction of PZT decreased. The optimum dielectric properties were observed for the $x = 0.5$ composition with a permittivity of 22,000 and P_s, P_r, and E_c values of 31.9 μC/cm^2, 25.2μC/cm^2, and 4.0 kV/cm, respectively.

REFERENCES

1. L.E. Cross, Ferroelectrics **76,** 241 (1987).
2. T.R. Shrout and A. Halliyal, Am. Ceram. Soc. Bull. **66,** 704 (1987).
3. K. Uchino, Ferroelectrics **151,** 321 (1994).
4. K. Uchino, Solid State Ionics **108,** 43 (1998).
5. K. Uchino, *Ferroelectric Devices* (Marcel Dekker, New York, 2000).
6. K. Uchino, *Piezoelectric Actuators and Ultrasonic Motors* (Kluwer Academic Publishers, Boston, MA, 1996).
7. V.A. Bokov and I.E. Mylnikova, Sov. Phys-Solid State **2,** 2428 (1960).
8. J. Kuwata, K. Uchino, and S. Nomura, Ferroelectrics **37,** 579 (1981).
9. K. Uchino, Ceram. Int. **21,** 309 (1995).
10. S.E. Park and T.R. Shrout, IEEE Tr. UFFC. **44,** 1140 (1997).
11. M.L. Mulvihill, L.E. Cross, W. Cao, and K. Uchino, J. Am. Ceram. Soc. **80,** 1462 (1997).
12. C.A. Randall and A.S. Bhalla, Jpn. J. Appl. Phys. **29,** 327 (1990).
13. A.S. Bhalla, R. Guo, and R. Roy, Mat. Res. Innovat. **4,** 3 (2000).
14. N. Mizutani, N. Wakiya, K. Shinozaki, and N. Ishizawa, Mater. Res. Bull. **30,** 1121 (1995).
15. A. Halliyal, U. Kumar, R.E. Newham, and L.E. Cross, Am. Ceram. Soc. Bull. **66,** 671 (1987).
16. J.R. Belsick, A. Halliyal, U. Kumar, and R.E. Newnham, Am. Ceram. Soc. Bull. **66,** 664 (1987).
17. H.Q. Fan and H.E. Kim, J. Appl. Phys. **91,** 317 (2002).
18. H.Q. Fan and H.E. Kim, J. Mater. Res. **17,** 180 (2002).
19. V.A. Bokov and I.E. Myl'nikova, Sov. Phys. Solid State **3,** 631 (1961).
20. L. Veitch, Thesis, Pennsylvania State University (1982).
21. D. Luff, R. Lane, K.R. Brown, and H.J. Marshallsay, Trans. J. Brit. Ceram. Soc. **73,** 251 (1974).
22. O. Babushkin, T. Lindback, J.C. Luc, and J. Leblais, J. Eur. Ceram. Soc. **18,** 737 (1998).
23. S.H. Lee, H.G. Kim, H.I. Choi, and G. Sa-Gong, IEEE Int. Conf. Prop. Appl. Dielectric Mater. **2,** 1062 (1997).
24. S.L. Swartz and T.R. Shrout, Mater. Res. Bull. **17,** 1245 (1982).
25. G. Robert, M.D. Maeder, D. Damjanovic, and N. Setter, J. Am. Ceram. Soc. **84,** 2869 (2001).
26. S. Ananta, R. Tipakontitikul, and T. Tunkasiri, Mater. Lett. **4214,** 1 (2002).
27. JCPDS No. 25-0446 (International Center for Diffraction Data, Newton Square, PA, 2000).
28. H.M. Jang, S.R. Cho, and K.M. Lee, J. Am. Ceram. Soc. **78,** 297 (1995).
29. F. Xia and X. Yao, J. Mater. Sci. **36,** 247 (2001).
30. S.L. Swartz, T.R. Shrout, W.A. Schulze, and L. E. Cross, J. Am. Ceram. Soc. **67,** 311 (1984).
31. R.D. Shannon, Acta. Crystallogr. A **32,** 751 (1976).
32. T.R. Shrout, R. Eitel, and C.A. Randall, IEEE Tr. UFFC. **44,** 1140 (2002).
33. A.J. Moulson and J.M. Herbert, *Electroceramics: Materials, Properties, Applications* (Chapman and Hall, New York, 1990).
34. L.E. Cross, Ferroelectrics **151,** 305 (1994).
35. H. Fan, L. Zhang, L. Zhang, and X. Yao, J. Phys. Condens. Matter **12,** 4381 (2000).
36. D. Pandey, Key Eng. Mater. **101–102,** 177 (1995).
37. A. Vierheilig, A. Safari, and A. Halliyal, Ceram. Trans. **8,** 75 (1990).

Influence of processing conditions on the phase transition and ferroelectric properties of $Pb(Zn_{1/3}Nb_{2/3})O_3-Pb(Zr_{1/2}Ti_{1/2})O_3$ ceramics

Naratip Vittayakorn [a,*], Gobwute Rujijanagul [a], Tawee Tunkasiri [a], Xiaoli Tan [b], David P. Cann [b]

[a] *Department of Physics, Faculty of Science, Chiang Mai University, Chiang Mai 50200, Thailand*
[b] *Materials Science and Engineering Department, Iowa State University, Ames, IA 50011 USA*

Abstract

Ceramics solid solutions within the binary system of $xPb(Zn_{1/3}Nb_{2/3})O_3-(1-x)Pb(Zr_{1/2}Ti_{1/2})O_3$ with $x = 0.1$–0.5 were synthesized via the mixed oxide method and the columbite method. Phase development of calcined powders and the crystal structure of sintered ceramics were analyzed by X-ray diffraction. Ferroelectric properties were measured to elucidate the phase transformation and identify the impact of the processing conditions. It is shown that there was no significant difference in P_r across the composition range. However, the coercive field E_c was shown to exhibit a strong compositional dependence. Compared with ceramics prepared by the columbite method, ceramics prepared by the mixed oxide method showed a lower remanent polarization P_r and a higher coercive field E_c. In addition, both X-ray diffraction and ferroelectric measurements indicated a phase transformation from a tetragonal to a pseudo-cubic rhombohedral phase when the fraction of $Pb(Zn_{1/3}Nb_{2/3})O_3$ (PZN) was increased. The morphotropic phase boundary (MPB) is located between $x = 0.2$ and 0.3 according to observations made on ceramics prepared with the columbite method. However, this transformation was obscured in the ceramics prepared with the mixed oxide method. It is proposed that compositional heterogeneities were responsible for these experimental investigations.
© 2004 Elsevier B.V. All rights reserved.

Keywords: Phase transition; Ferroelectric properties; Ceramics

1. Introduction

Ferroelectric materials are widely used for various devices, including multilayer capacitors, sensors, and actuators. By the 1950s, the piezoelectric solid solution $Pb(Zr_{1-x}Ti_x)O_3$ (PZT) was found to host exceptionally high dielectric and piezoelectric properties for compositions close to the morphotropic phase boundary (MPB). This MPB is located around $PbTiO_3:PbZrO_3 \sim 1:1$ and separates the Ti-rich tetragonal phase from the Zr-rich rhombohedral phase [1]. Most commercial PZT ceramics are thus designed in the vicinity of the MPB with various dopings in order to achieve high properties.

$Pb(Zn_{1/3}Nb_{2/3})O_3$ (PZN) is an important relaxor ferroelectric material with the rhombohedral structure at room temperature. A diffuse phase transition from the paraelectric state to a ferroelectric polar state occurs at 140 °C [2]. Extensive research has been carried on PZN single crystals because of their excellent dielectric, electrostrictive, and optical properties [2,3]. Although single crystals of PZN can routinely be grown by the flux method, [4] it is known that perovskite PZN ceramics cannot be synthesized by the conventional mixed-oxide method without doping. This is because PZN has a low tolerance factor and small electronegativity difference between the cations and the pyrochlore phase appears to be more thermodynamically stable than the perovskite phase [5]. Attempts to synthesize perovskite PZN ceramics invariably results in the formation of pyrochlore phase with inferior dielectric and piezoelectric properties. The columbite method, as suggested by Schwartz and Shrout [6] for the prepa-

* Corresponding author. Tel.: +1-515-294-3801;
fax: +1-515-294-5444.

E-mail address: naratip@iastate.edu (N. Vittayakorn).

ration of perovskite $Pb(Mg_{1/3}Nb_{2/3})O_3$ (PMN) ceramic, is not effective in suppressing pyrochlore phase formation in PZN ceramics [5]. Hot isostatic pressing was reported to be able to produce phase-pure perovskite PZN ceramics [7]. However, relatively poor piezoelectric properties were measured in the as-pressed ceramic. Various chemical additives, such as $Ba(Zn_{1/3}Nb_{2/3})O_3$, $BaTiO_3$, and $SrTiO_3$ have thus been explored in an attempt to stabilize the perovskite PZN ceramic and retain the excellent piezoelectric properties. Halliyal et al. [8] prepared $BaTiO_3$-stabilized PZN ceramics using $BaCO_3$, PbO, ZnO, Nb_2O_5, and TiO_2 as the starting materials. Villlegas et al. [9] incorporated $BaTiO_3$ and $Pb(Zr_{0.4}Ti_{0.6})O_3$ into PZN to produce the ternary system with the perovskite structure from $ZnNb_2O_6$ powder. However, a trade-off was made with these additives which yielded reduced dielectric constants and piezoelectric coefficients. Therefore, there is significant interest in finding a method to stabilize the perovskite phase in PZN without sacrificing the excellent dielectric and piezoelectric properties.

Since both PZT and PZN have perovskite structure and are known to have excellent dielectric and piezoelectric properties, it is suggested to alloy PZN with PZT to stabilize and optimize the PZN ceramics. Recent work by Fan and Kim [10] has shown promise in producing phase-pure perovskite PZN–PZT ceramics with the conventional mixed-oxide method. The present work aims to provide a comprehensive study on the process-property relationships in the binary system of PZN–PZT with a wide composition range. Both the conventional mixed-oxide method and the columbite precursor method have been used in synthesizing the PZN–PZT ceramics. The conventional method utilized a one-step reaction with all of starting materials whereas the columbite method was used an initial step of preparing columbite precursor ($ZnNb_2O_6$) and wolframite precursor ($ZrTiO_4$) followed by a reaction with PbO to form the PZN–PZT ceramics. Finally, a comparison of the important ferroelectric properties was made to identify the optimum processing conditions.

2. Experimental procedure

For the conventional method, regent grade oxides of PbO, ZnO, ZrO_2, TiO_2 and Nb_2O_5 were mixed in the required stoichiometric ratios for the general composition xPZN–$(1-x)$PZT where $x = 0.1, 0.2, 0.3, 0.4$, and 0.5. After ball milling for 24 h and drying at 120 °C, the mixture was calcined at temperatures between 750 and 950 °C for 4 h in a double crucible configuration [11]. A heating rate of 20 °C/min was selected for all of the compositions in this system [11]. For the columbite method, the columbite precursor $ZnNb_2O_6$ was prepared from the reaction between ZnO (99.9%) and Nb_2O_5 (99.9%) at 975 °C for 4 h. The wolframite precursor $ZrTiO_4$ was formed by reacting ZrO_2

(99.9%) with TiO_2 (99.9%) at 1400 °C for 4 h. The precursors $ZnNb_2O_6$, $ZrTiO_4$ were then subsequently mixed with PbO (99.9%) (with 2 mol% excess PbO) [11] and milled, dried, and calcined under the same conditions as the powder prepared by conventional method. The calcined powders of both methods were cold isostatically pressed into pellets at a pressure of 150 MPa. Five sintering conditions were selected to be used with both methods ranging 1175, 1200, 1225, 1250, and 1275 °C dwell 2 h. To prevent PbO volatilization from the pellets, a PbO atmosphere was controlled with a bed of $PbZrO_3$ powder placed in the vicinity of the pellets. The calcined powder and sintered pellets were checked for perovskite phase formation by X-ray diffraction (XRD). Data collection was performed in the 2θ range of 20°–60° with a step scan with a step size of 0.02° and counting time of 2 s per step. For profile fitting, a step scan
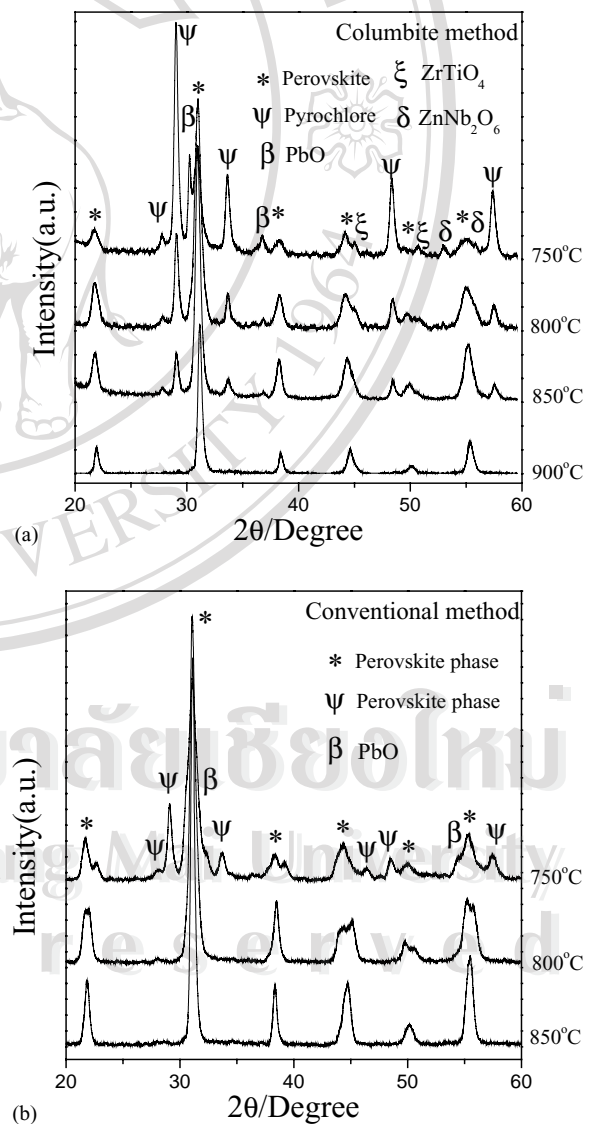

Fig. 1. XRD patterns for 0.3PZN–0.7PZT ceramics calcined at varies temperature for 4 h. (a) Columbite method; (b) conventional method.
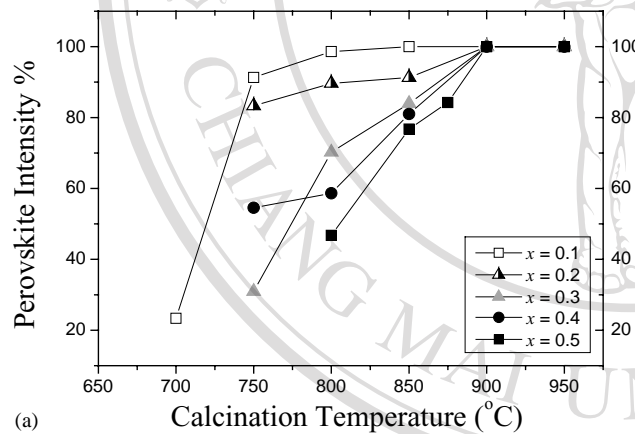
with step size of $0.004°$ was used with a counting time of 5 s per step and peak deconvolution was done with JADE v.6.

The relative amounts of perovskite and pyrochlore phases were approximated by calculating the ratio of the major XRD peak intensities of the perovskite and pyrochlore phase via the following equation:
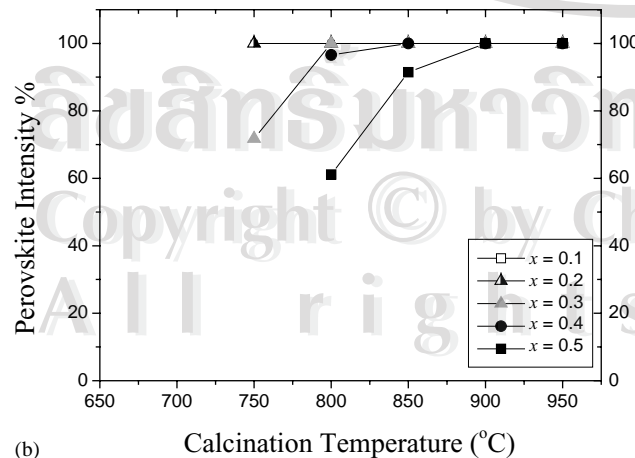
$$\text{Perovskite intensity (\%)} = \left(\frac{I_{\text{perov}}}{I_{\text{perov}} + I_{\text{pyro}} + I_{\text{PbO}}} \right) \times 100$$

where I_{perov}, I_{pyro}, and I_{PbO} refer to the intensity of the (1 1 0) perovskite peak, (2 2 2) pyrochlore peak, and the intensity of the highest lead oxide peak, respectively.

To investigate the influence of post-sintering heat treatments, specimens from both methods which had been sintered at $1175°C$ were annealed at $1250°C$ for a dwell time of 6 h in a closed Al_2O_3 crucible with PbO-rich atmosphere. The specimens were polished and electroded via gold sputtering, over which a layer of air-dry silver paint was applied to enhance the electrical contact. The ferroelectric polarization versus electric field (*P–E*) measurements was made using an RT66A standard ferroelectric test system.
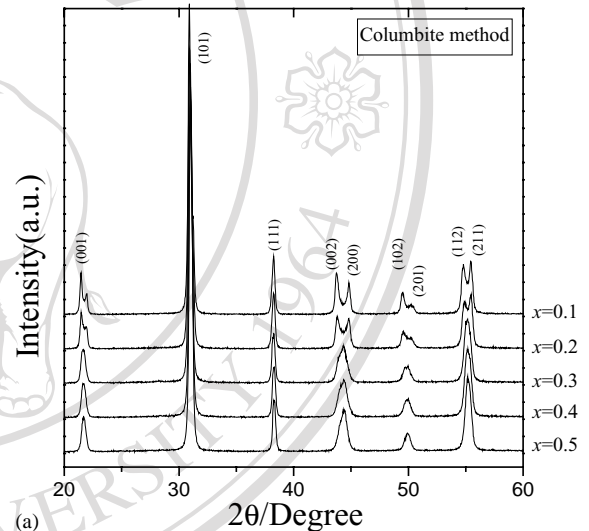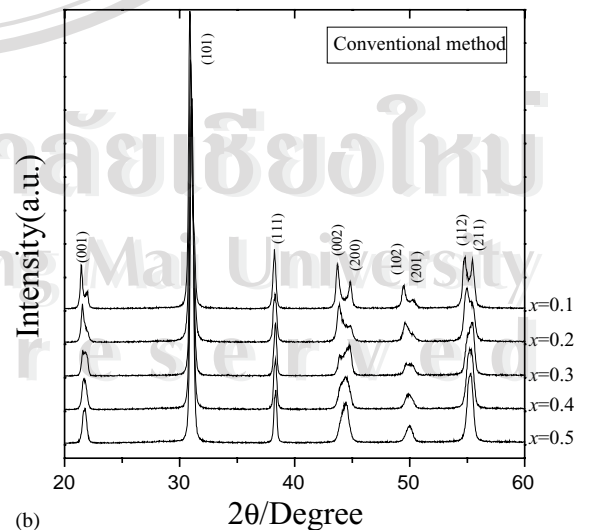
3. Results and discussion

3.1. Perovskite phase formation and the MPB

Powder XRD patterns of the calcined 0.3PZN–0.7PZT powders at different calcination temperatures for both methods are shown in Fig. 1(a) and (b). The XRD results show that the pyrochlore phase $Pb_{1.88}(Zn_{0.3}Nb_{1.25})O_{5.305}$ (JCPDS No. 25-0446) was dominant at calcination temperatures below $750°C$ for all of the columbite-derived powders. The precursor phases PbO, $ZrTiO_4$, $ZnNb_2O_6$ were also detected by XRD at below $800°C$. No evidence of the precursor phase ZrO_2, TiO_2, Nb_2O_5 or ZnO was detected by XRD for conventional preparation. Moreover, the pyrochlore phase was only observed in the conventional method-derived powders for compositions with a high concentration of lead zinc niobate. It is assumed that the columbite phase $ZnNb_2O_6$

Fig. 2. Percentage of perovskite phase as a function of calcination temperature for *x*PZN–(1 − *x*)PZT ceramics: (a) columbite method; (b) conventional method.

Fig. 3. XRD patterns for *x*PZN–(1 − *x*)PZT ceramics sintered at $1200°C$ for 2 h: (a) columbite method; (b) conventional method.
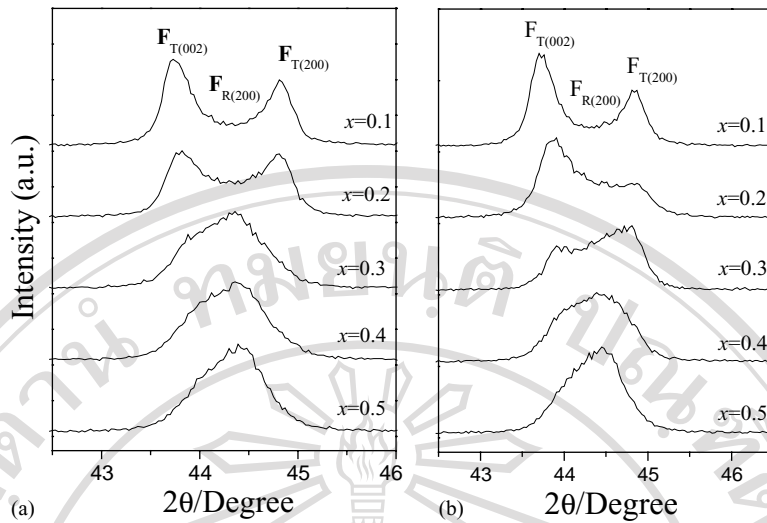
Fig. 4. Close examination of the (0 0 2) peaks shown in Fig. 2. (a) Columbite method; (b) conventional method.

decomposed via reaction with PbO at low temperatures to form the pyrochlore phase $Pb_{1.88}(Zn_{0.3}Nb_{1.25})O_{5.305}$. For the conventional method, $Pb_xNb_yO_z$ pyrochlore phases were found at calcination temperatures below 800 °C for $x > 0.3$. In the work by Chen et. al. [12] it was reported that in

the lead-niobium pyrochlore system the cubic $Pb_3Nb_4O_{13}$, pyrochlore phase (JCPDS No. 25–443) forms first around 580 °C. At higher temperatures, it transforms to $Pb_2Nb_2O_7$, (JCPDS No. 40–828) and finally to $Pb_3Nb_2O_{8,}$ (JCPDS No. 30–712) with increased calcination temperatures. At
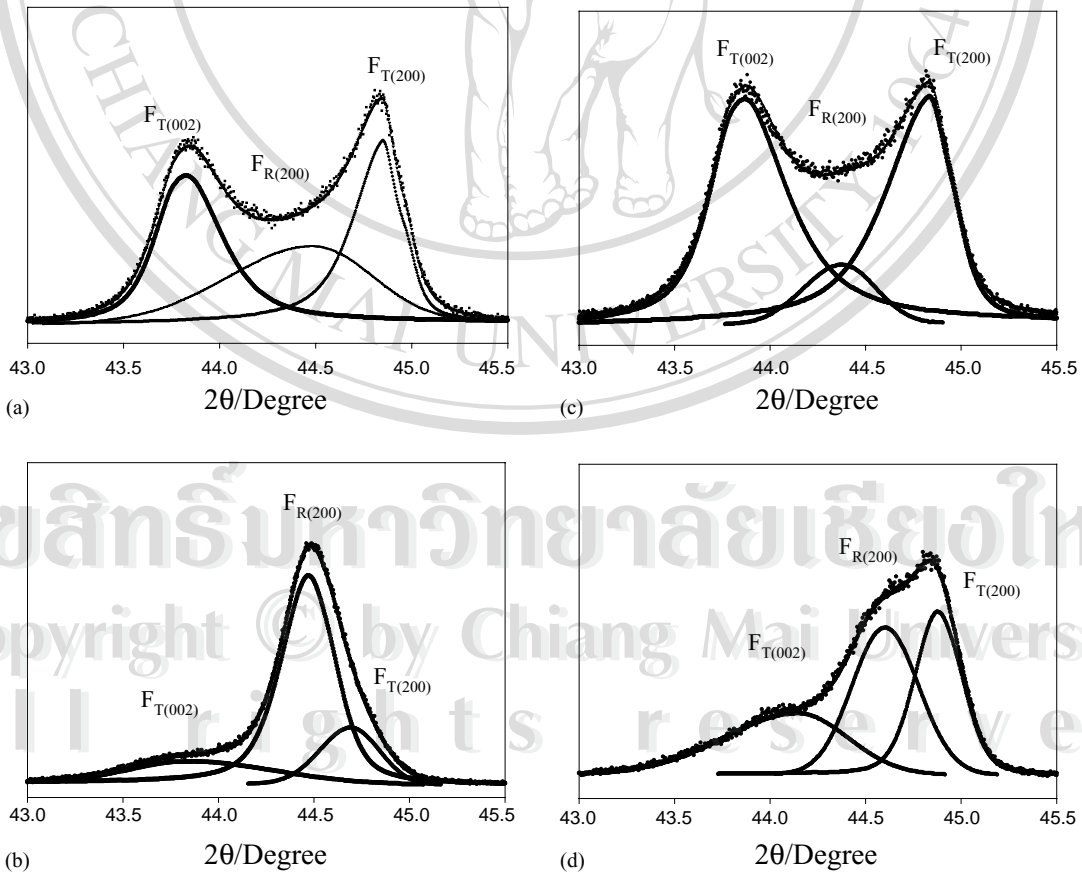

Fig. 5. Individual X-ray diffraction (0 0 2) peak for the tetragonal ($F_{T(0 0 2)}$, $F_{T(2 0 0)}$) and rhombohedral($F_{R(2 0 0)}$) phase for difference methods, (a) 0.2PZN–0.8PZT prepared by columbite method, (b) 0.3PZN–0.7PZT prepared by columbite method, (c) 0.2PZN–0.8PZT prepared by conventional method, (d) 0.3PZN–0.7PZT prepared by conventional method.

800 °C, the pyrochlore phase began to decrease and disappeared completely at 850 °C for powder prepared by conventional method and at 900 °C for the columbite method. The optimum calcination temperature for the formation of phase pure perovskite was found to be about 850 °C for the conventional method and 900 °C for the columbite method.

The perovskite phase formation for both processing methods at various calcination temperatures is shown in Fig. 2(a) and (b), respectively. All the compositions from both methods in the present work showed pyrochlore-free XRD scans at calcination temperatures at above 900 °C. These experiments indicate that for both methods as the concentration of the PZN phase increased the calcination temperature must be increased in order to obtain phase-pure perovskite. Most processing procedures for PZN-based ceramics make use of calcination temperatures in excess of 900 °C. The experiments in this study suggest that the conventional method helps to stabilize the perovskite phase compared with the columbite method. Moreover the perovskite formation temperature for the conventional method was significantly lower than that of the columbite method. The difference in the formation temperatures was presumably due to a different reaction path to the formation of the perovskite phase for the two methods.

Fig. 3 shows the XRD patterns of xPZN–$(1 - x)$PZT ceramics sintered at 1200 °C for 2 h to illustrate the change in crystal structure as a function of composition for both processing methods. The results indicate that, for the same composition, different processing methods may develop a perovskite structure with different symmetries. Fig. 4 shows the evolution of the (2 0 0) peak as a function of composition and processing method. The PbZrO$_3$–PbTiO$_3$ phase diagram predicts that at room temperature Pb(Zr$_{1/2}$Ti$_{1/2}$)O$_3$ falls within the tetragonal phase field near the MPB. The XRD patterns with low PZN concentration show strong (2 0 0) peak splitting which is indicative of the tetragonal phase. As the PZN concentration increased, for both processing methods the (2 0 0) transformed to a single peak which suggests rhombohedral symmetry.

Fig. 5(a–d) show the XRD patterns for both processing methods in the vicinity of the MPB at $x = 0.2$ and 0.3 over the range $2\theta = 43$–45.5. The data shows the appearance of a triplet peak due to the superposition of the tetragonal and rhombohedral (2 0 0) peaks. The columbite prepared samples show a relatively sharp transition between the tetragonal phase at $x = 0.2$ to the rhombohedral phase at $x = 0.3$. In the conventional prepared samples, while the $x = 0.2$ samples shows the presence of the tetragonal phase there is a strong co-existence of both phases for the $x = 0.3$ pattern.

While Fan and Kim report a phase boundary in the same PZN–PZT system at the composition $x = 0.5$, [13] there are no prior reports of the phase boundary observed in this work between $x = 0.2$ and 0.3.
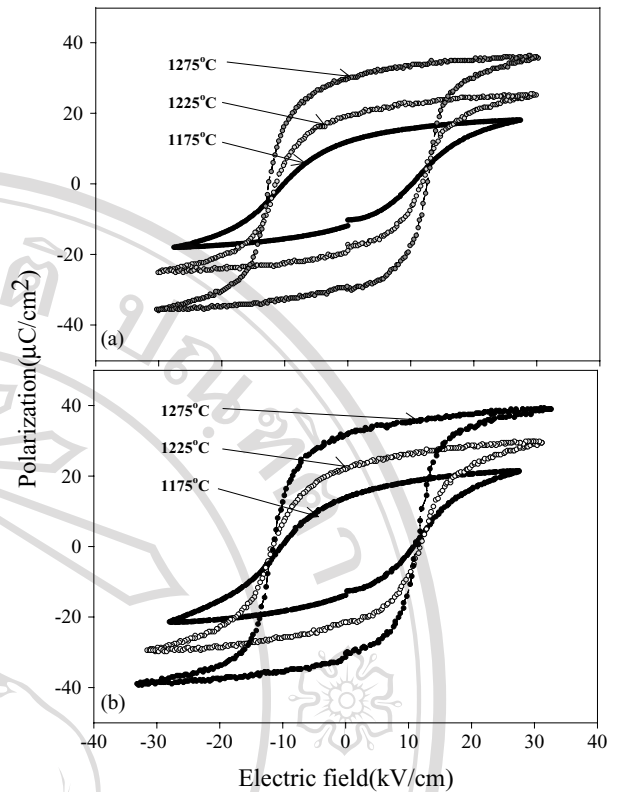

Fig. 6. Room temperature *P–E* hysteresis as a function of sintering temperature for 0.2PZN—0.8PZT: (a) columbite method; (b) conventional method.

3.2. Effect of sintering temperature and post-sinter annealing

The effect of sintering temperature on the properties was assessed by the polarization–field (*P–E*) measurements. Fig. 6 shows the results for the composition of $x = 0.2$ for both methods at different sintering temperatures. Ceramics from both methods showed normal ferroelectric behavior with a rectangular loop. The remanent polarization, P_r, was observed to increase with increasing sintering temperature. This is probably due to the smaller grain size at low sintering temperature. This may result in a smaller domain size, and furthermore domain wall motion in smaller grains is subject to stricter constraints [1]. Strong internal stresses are expected in fine-grained specimens and polarization switching is thus greatly suppressed. This was accompanied by the decrease in the coercive field with increasing sintering temperature [14].

For compositions with $x > 0.3$, the P_r decreased at high sintering temperatures. For the composition of $x = 0.1$, rectangular hysteresis loops were not observed even at a sintering temperature of 1250 °C, as shown in Fig. 7. It has been reported that post-sinter annealing is effective in improving the dielectric and ferroelectric properties of lead-based ceramics [15]. Specimens for each composition sintered at the lowest temperature (1175 °C) were annealed at 1250 °C for 6 h. Indeed, significant improvements of
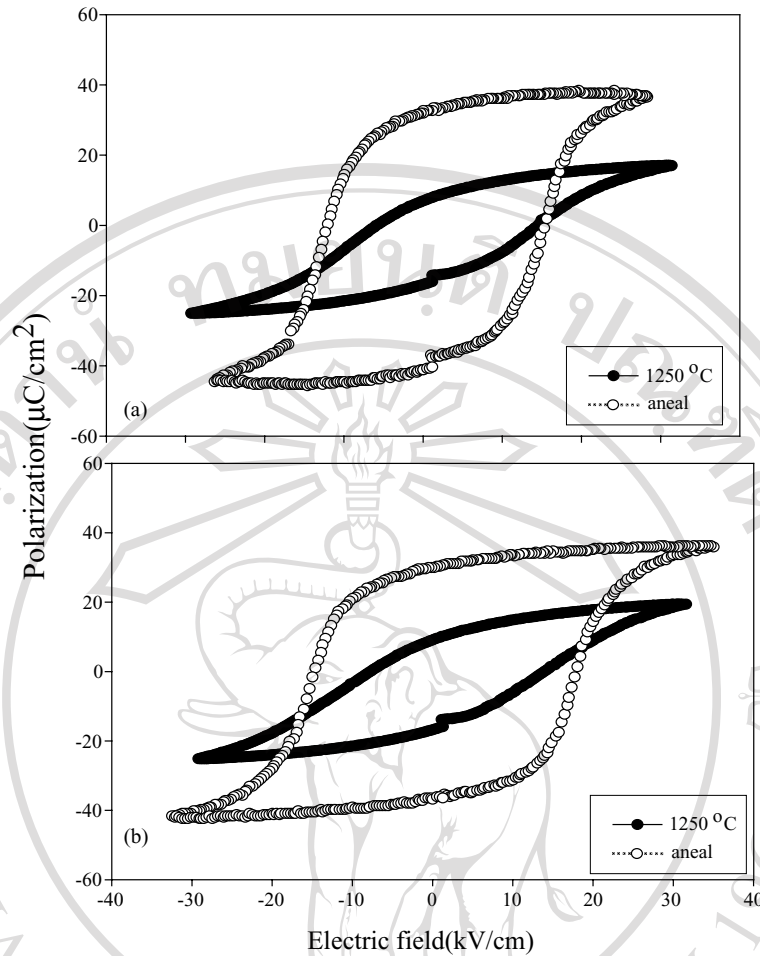
Fig. 7. Effect of post-sinter annealing on the *P–E* hysteresis for 0.1PZN–0.9PZT ceramics: (●) sintered at 1250 °C, (○) sintered at 1175 °C and annealed at 1250 °C for 6 h: (a) columbite method, (b) conventional method.

the ferroelectric properties were demonstrated (see Fig. 7 for the 0.1PZN–0.9PZT). The results on other compositions are listed Table 1. Very limited improvements were observed for the $x = 0.5$ composition because the higher PZN content required lower sintering temperatures, thus limiting the efficacy of the annealing step. It has been suggested that PZT ceramics should be sintered at temperatures above 1200 °C [8,9,16] and PZN-based ceramics should

be sintered below this temperature [17] to achieve the best combination of density and properties. This explains the results in our present study where increasing molar fraction of PZN directly led to a lower sintering temperature. Therefore, post-sinter heat treatment is not necessary for ceramics with high PZN content.

Based on these ferroelectric measurements, the optimum sintering conditions for compositions of $x = 0.3$, 0.4, and

Table 1
Post-sinter annealing effects on the remanent polarization P_r and saturation polarization P_s in xPZN–$(1 − x)$PZT ceramics sintered at 1175 °C for 2 h and annealed at 1250 °C for 6 h

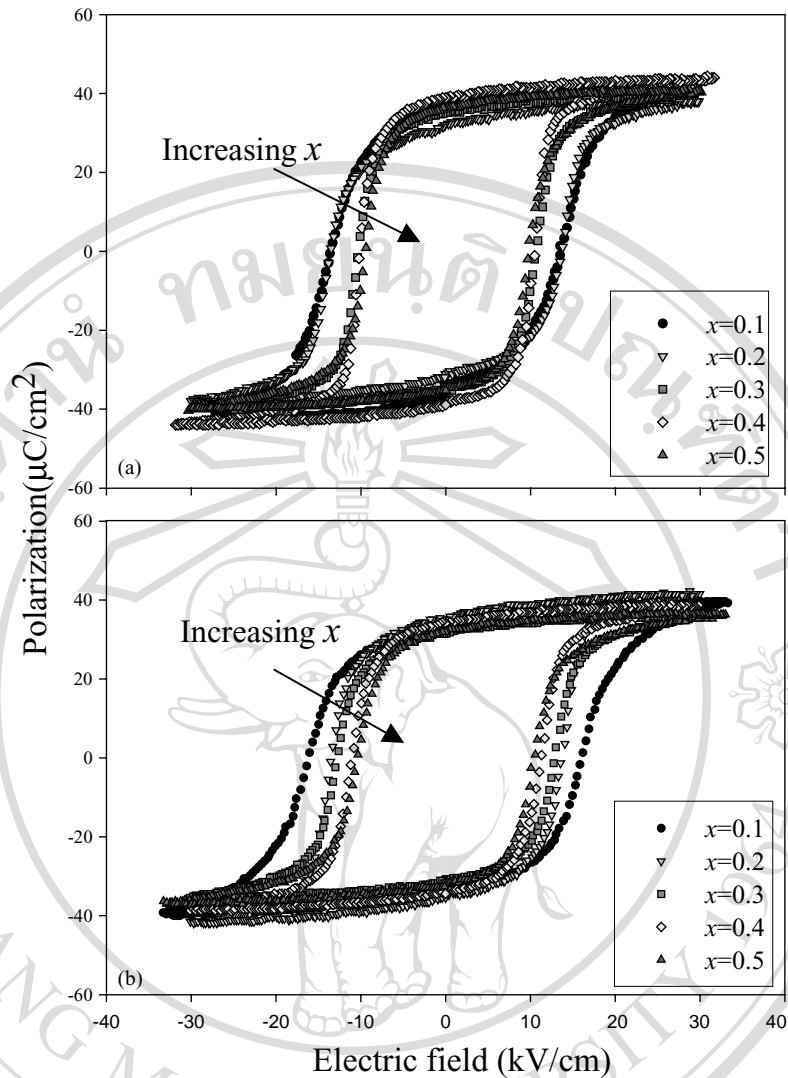| x	xPZN−$(1 − x)$PZT							
	Columbite method				Conventional method			
	P_r		P_s		P_r		P_s	
	Sintered	Annealed	Sintered	Annealed	Sintered	Annealed	Sintered	Annealed
0.1	7.6	37.1	15.8	42.9	9.4	34	19.0	39.2
0.2	14.6	36.1	20.6	38.9	13.8	31.5	21.4	35.0
0.3	31.9	30.4	37.2	33.5	23.8	20.0	27.9	23.2
0.4	32.3	30.6	35.8	34.5	30.5	23.2	35.0	28.7
0.5	35.6	36.4	40.4	42.1	29.4	29.5	34.5	34.9

Fig. 8. Effect of composition (x) on the *P–E* hysteresis loops for xPZN–$(1 - x)$PZT processed at the optimum processing conditions: (a) columbite method; (b) conventional method.

0.5 is 1200 °C for 2 h. The sintering process was not completed at these sintering conditions for compositions of $x =$ 0.1 and 0.2 and therefore post-sinter annealing at 1250 °C for 6 h is necessary for improvement of ferroelectric properties. Further characterization techniques and comparisons, which are described in the following section, were made on these as-sintered specimens (for $x =$ 0.3, 0.4, 0.5) and annealed specimens (for $x =$ 0.1, 0.2) because they were found to have the optimum ferroelectric properties.

3.3. Effect of processing method on the phase transformation

The *P–E* ferroelectric property measurements for the specimens processed at optimum conditions are summarized in Fig. 8. It is shown that there is no significant difference in P_r across the composition range. However, the coercive field E_c is well dispersed over the compositions. This is further illustrated in Fig. 9. Compared to the conventional method, columbite method produces a slightly higher remanent polarization P_r as well as a lower coercive field E_c. Both methods show a considerable decrease in E_c with increasing molar fraction of PZN. However, the variation in ceramics prepared by conventional method is gradual and continuous, while an abrupt change in E_c occurs in ceramics processed by the columbite method, as indicated in Fig. 9(b). Combined with the XRD examination described in Section 3.1, the change in E_c clearly indicates a phase transformation over that compositional range. Therefore, an MPB separating the tetragonal phase (PZT-rich) from the pseudo-cubic rhombohedral phase (PZN-rich) exists between $x =$ 0.2 and 0.3. Also consistent with the XRD data, the phase transformation in ceramics prepared by the conventional method is smeared out due probably to the chemical heterogeneities. These results lead to the conclusion that the columbite method produces ceramics with bet-
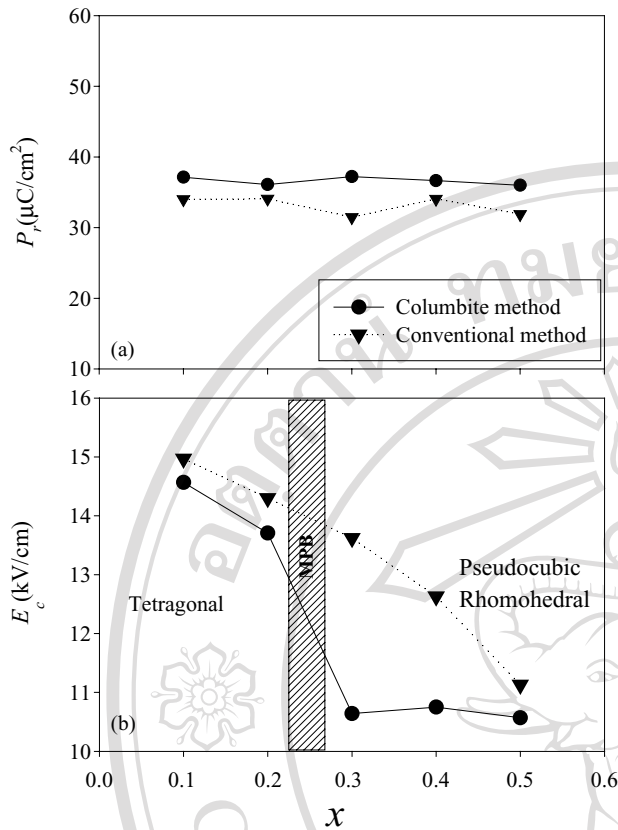
Fig. 9. Variation of remanent polarization P_r and coercive field E_c with composition for xPZN–$(1 - x)$PZT ceramics: (a) remanent polarization; (b) coercive field.

ter ferroelectric properties even though this method seems initially be prone to form pyrochlore phase. These results underscore the important role that B-site ordering plays in determining the thermodynamic stability and electrical properties of perovskite ferroelectrics.

4. Conclusion

A comparison between the conventional method and the columbite method was made in the preparation of ceramics within the solid solution of xPZN–$(1 - x)$PZT over a wide range in composition ($x = 0.1$–0.5). The optimum processing conditions for excellent ferroelectric properties were identified. Based on the X-ray structural analysis and ferroelectric property measurements, the following conclusions can be drawn:

1. Compared to the columbite method, the conventional method requires lower calcination temperature to eliminate the pyrochlore phase formation. Increasing in the molar fraction of PZN requires increased calcination temperatures in order to achieve phase-pure perovskite. At 900 °C, all the compositions for both methods can be converted to single-phase perovskite.

2. In ceramics sintered from columbite method prepared powders, a sharp transition from tetragonal to pseudo-cubic rhombohedral phase was evidenced by the XRD analysis. Thus, an MPB exists between $x = 0.2$ and 0.3. However, such a phase transformation is diffuse in ceramics prepared by the conventional method.
3. The results from XRD analysis are consistent with the ferroelectric property measurements. An abrupt change in coercive field, E_c, was observed in ceramics prepared by the columbite method at the same composition range of $x = 0.2$–0.3. In contrast, gradual change was found in ceramics prepared by the conventional method.
4. Lower sintering temperatures were required for compositions with an increasing molar fraction of PZN. For the $x = 0.1$ and 0.2 compositions, sintering at 1250 °C for 2 h was observed to produce inferior ferroelectric properties and post-sinter annealing was required to achieve excellent ferroelectric properties.
5. For both methods, no considerable variation of the remanent polarization with compositions was observed. However, the coercive field was observed to decrease with increasing amount of PZN. The columbite method was found to produce ceramics with better ferroelectric properties with higher remanent polarization and lower coercive field.

References

[1] A.J. Moulson, J.M. Herbert, Electroceramics: Materials, Properties, Appications, Chapman and Hall, New York, 1990.
[2] K. Uchino, Solid State Ionics 108 (1998) 43.
[3] K. Uchino, Ferroelectrics 151 (1994) 321.
[4] V.A. Bokov, I.E. Mylnikova, Sov. Phys-Solid state 2 (1960) 2428.
[5] T.R. Shrout, A. Halliyal, Am. Ceram. Soc. Bull. 66 (1987) 704–711.
[6] S.L. Swartz, T.R. Shrout, Mater. Res. Bull. 17 (1982) 1245–1250.
[7] Y. Matsuo, H. Sasaki, S. Hayakawa, F. Kanamaru, M. Koizumi, J. Am. Ceram. Soc. 52 (1969) 516–517.
[8] A. Halliyal, U. Kumar, R.E. Newham, L.E. Cross, Am. Ceram. Soc. Bull. 66 (1987) 671–676.
[9] M. Villegas, A.C. Caballero, C. Moure, R.E. Newham, J. Am. Ceram. Soc. 83 (2000) 141.
[10] H. Fan, H.-E. Kim, J. Mater. Res. 17 (2002) 180.
[11] N. Vittayakorn, G. Rujijanagul, T. Tunkasiri, X. Tan, D.P. Cann, J. Mater. Res. 18 (2003) 2882–2889.
[12] S.-Y. Chen, C.-M. Wang, S.-Y. Cheng, Mater. Chem. Phys. 49 (1997) 70–77.
[13] H. Fan, H.-E. Kim, J. Appl. Phys. 91 (2002) 317.
[14] U. Kenji, Ferroelectric Devices, Marcel Dekker Inc., 2000.
[15] F. Xia, X. Yao, J. Mater. Sci. 36 (2001) 247.
[16] J.R. Belsick, A. Halliyal, U. Kumar, R.E. Newnham, Am. Ceram. Soc. Bull. 66 (1987) 664.
[17] A. Halliyal, A. Safari, Ferroelectrics 158 (1994) 295–300.

The morphotropic phase boundary and dielectric properties of the xPb(Zr$_{1/2}$Ti$_{1/2}$)O$_3$-(1 − x)Pb(Ni$_{1/3}$Nb$_{2/3}$)O$_3$ perovskite solid solution

Naratip Vittayakorn and Gobwute Rujijanagul
Department of Physics Faculty of Science, Chiang Mai University, Chiang Mai 50200, Thailand

Xiaoli Tan, Meagen A. Marquardt, and David P. Cann
Materials Science and Engineering Department, Iowa State University, Ames, Iowa 50011

The solid solution between the normal ferroelectric Pb(Zr$_{1/2}$Ti$_{1/2}$)O$_3$ (PZT) and relaxor ferroelectric Pb(Ni$_{1/3}$Nb$_{2/3}$)O$_3$ (PNN) was synthesized by the columbite method. The phase structure and dielectric properties of xPZT-(1−x)PNN where $x=0.4–0.9$ and the Zr/Ti composition was fixed close to the morphotropic phase boundary (MPB) were investigated. With these data, the ferroelectric phase diagram between PZT and PNN has been established. The relaxor ferroelectric nature of PNN gradually transformed towards a normal ferroelectric state towards the composition 0.7PZT-0.3PNN, in which the permittivity was characterized by a sharp peak and the disappearance of dispersive behavior. X-ray diffraction analysis demonstrated the coexistence of both the rhombohedral and tetragonal phases at the composition 0.8PZT-0.2PNN, a new morphotropic phase boundary within this system. Examination of the dielectric spectra indicates that PZT-PNN exhibits an extremely high relative permittivity near the MPB composition. The permittivity shows a shoulder at the rhombohedral to tetragonal phase transition temperature $T_{RT}=195$ °C, and then a maximum permittivity (36 000 at 10 kHz) at the transition temperature $T_{max}=277$ °C at the MPB composition. The maximum transition temperature of this system was 326 °C at the composition $x=0.9$ with the relative permittivity of 32 000 at 10 kHz. © *2004 American Institute of Physics*.
[DOI: 10.1063/1.1796511]

I. INTRODUCTION

The relaxor ferroelectric lead nickel niobate [Pb(Ni$_{1/3}$Nb$_{2/3}$)O$_3$, PNN] has been studied by numerous researchers since its discovery by Smolenskii and Agranovskaya in 1958.[1] At room temperature, single crystal PNN has the cubic prototype symmetry $Pm3m$ with a lattice parameter (a)$=4.03$ Å.[2] Nanometer-level chemical heterogeneity in the form of short range ordering of Ni^{2+} and Nb^{5+} on the B site was proposed to account for the diffuse phase transition.[3] The complex perovskite shows a broad maximum of the dielectric permittivity near −120 °C with relative permittivity near 4000 at 1 kHz.[4]

In the last decade, normal ferroelectric lead zirconate titanate [Pb(Zr$_{1-x}$Ti$_x$)O$_3$, PZT] has become one of the most important commercially produced piezoelectric materials.[5,6] Excellent piezoelectric properties have been observed in compositions close to the morphotropic phase boundary (MPB Zr:Ti ~52:48).[5–7] Recently, many piezoelectric ceramic materials have been developed from binary systems containing a combination of relaxor and normal ferroelectric materials[8] which yield high dielectric permittivities (e.g., Pb(Mg$_{1/3}$Nb$_{2/3}$)O$_3$-PbTiO$_3$,[9] Pb(Zn$_{1/3}$Nb$_{2/3}$)O$_3$-PbTiO$_3$,[10,11] Pb(Mg$_{1/3}$Nb$_{2/3}$)O$_3$-Pb(Zr,Ti)O$_3$,[12] excellent piezoelectric coefficients (e.g., Pb(Zn$_{1/3}$Nb$_{2/3}$)O$_3$-PbTiO$_3$,[10,11] Pb(Zn$_{1/3}$Nb$_{2/3}$)O$_3$-Pb(Zr,Ti)O$_3$,[13] Pb(Sc$_{1/2}$Nb$_{1/2}$)O$_3$-PbTiO$_3$[14,15] and high pyroelectric coefficients (e.g., Pb(Ni$_{1/3}$Nb$_{2/3}$)O$_3$-PbTiO$_3$-PbZrO$_3$).[16]

Fan and Kim[13] investigated the solid solution within the PZN-PZT binary system in which the Zr/Ti composition was close to the MPB. This study indicated that the composition 0.5PZN-0.5PZT showed the optimal piezoelectric properties. Moreover, these properties could be improved by thermal treatments. In 1974 Luff *et al.*[16] investigated solid solution in the Pb(Ni$_{1/3}$Nb$_{2/3}$)O$_3$-PbZrO$_3$-PbTiO$_3$ ternary system and observed excellent piezoelectric properties at the composition 0.5Pb(Ni$_{1/3}$Nb$_{2/3}$)O$_3$-0.35PbTiO$_3$-0.15PbZrO$_3$. There have been numerous papers published dealing with piezoelectric and processing issues within this compositional family.[16–19] These compositions have found wide applications and are now commercially available. However, there is limited information in the literature on the PNN-PZT system with Zr/Ti close to the MPB. Detailed reaction kinetics using conventional solid state processing of Pb(Ni$_{1/3}$Nb$_{2/3}$)O$_3$-Pb(Zr$_{0.48}$Ti$_{0.52}$)O$_3$ was recently investigated by Babushkin *et al.*.[20] A sequence of pyrochlore phases were detected at different temperatures, but there is no information pertaining to the dielectric and ferroelectric properties.

Since PNN is a relaxor ferroelectrics with a broad dielectric peak near $T_c \approx -120$ °C and PZT (Zr/Ti=50/50) is a normal ferroelectric with a sharp maximum permittivity at $T_c \sim 390$ °C, the curie temperature in PNN-PZT system can be engineered over a wide range of temperature by controlling the amount of PZT in the system. The aim of this work was to investigate the quasibinary solid solution xPZT (Zr/Ti=50/50)-(1−x)PNN, with $x=0.4–0.9$. Figure 1 schematically shows the pseudoternary composition range which
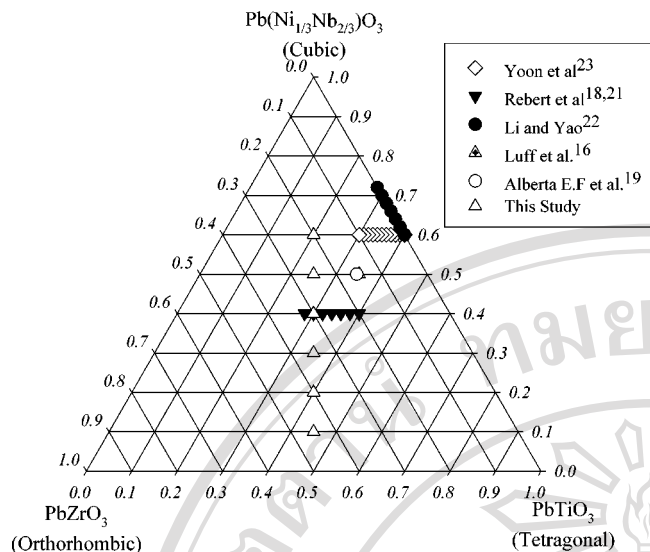
5103   © 2004 American Institute of Physics

FIG. 1. Compositions studied in the $Pb(Ni_{1/3}Nb_{2/3})O_3$-$PbZrO_3$-$PbTiO_3$ ternary system.

FIG. 2. XRD patterns at room temperature for xPZT-$(1-x)$PNN ceramics.

was studied in this work compared with other studies.[16,19–23] Although pure $Pb(Ni_{1/3}Nb_{2/3})O_3$-$PbZrO_3$-$PbTiO_3$ ternary ceramics can be fabricated by conventional methods,[16] the *B*-site precursor method is a better method for enhancing the dielectric properties and ferroelectric properties. This process involves prereacting the *B*-site cations to form the columbite phase $NiNb_2O_6$ and the wolframite phase $ZrTiO_4$. With this method it is possible to obtain a homogeneous perovskite solid solution without the other constituent perovskite phases such as $PbZrO_3$, $PbTiO_3$, PZT, PNN, and the formation of the parasitic pyrochlore phases is prevented. Finally, the nature of the relaxor-normal ferroelectric phase transition was studied through a combination of dielectric measurements and x-ray diffraction.

II. EXPERIMENT

The powders of xPZT-$(1-x)$PNN were synthesized using the columbite precursor method. Reagent-grade oxide powders of PbO, ZrO_2, TiO_2, NiO, and Nb_2O_5 were used as raw materials. The columbite structure ($NiNb_2O_6$) and wolframite structure ($ZrTiO_4$) were synthesized first. Stoichiometric amounts of the precursors (NiO, Nb_2O_5) and (ZrO_2, TiO_2) were mixed and milled in ethyl alcohol for 6 h using a vibratory mill. The mixture was dried at 60 °C for 12 h. The precursors $NiNb_2O_6$ and $ZrTiO_4$ were calcined at 975 °C and 1400 °C, respectively, for 4 h in a closed alumina crucible. The calcined $NiNb_2O_6$ and $ZrTiO_4$ powders were mixed with PbO in a stoichiometric ratio to form the composition xPZT-$(1-x)$PNN, where $x=0.4–0.9$ (shown in Fig. 1). In all compositions, 2 mol % excess PbO was added to compensate for lead volatilization during calcination and sintering. After remilling and drying, the mixtures were calcined at 950 °C for 4 h in a double alumina crucible configuration with a heating rate of 10 °C/min.

The calcined powders were milled for 3 h for reduced particle size. After grinding and sieving, the calcined powder was mixed with 5 wt % poly(vinyl alcohol) binder and uniaxially pressed into a pellet. Binder burnout occurred by
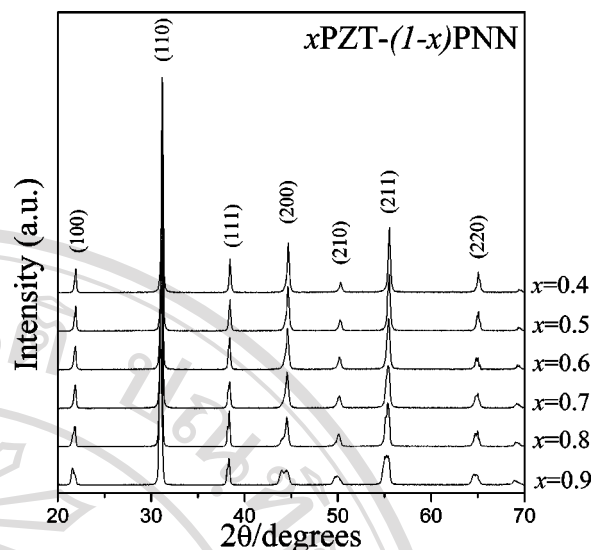
slowly heating to 500 °C and holding for 2 h. Sintering occurred between 1100–1250 °C with a dwell time of 4 h. To mitigate the effects of lead loss during sintering, the pellets were sintered in a closed alumina crucible containing $PbZrO_3$ powder.

The perovskite phase was examined by x-ray diffraction (XRD). Data collection was performed in the 2θ range of 20°–70° using step scanning with a step size of 0.02° and counting time of 2 s/step.

After surface grinding, the samples were electroded using sputtered gold and air-dried silver paint. The relative permittivity (ε_r) and dissipation factor (tan δ) were measured using an automated measurement system. This system consisted of an LCR meter (HP-4284A, Hewlett-Packard Inc.) in connection with a Delta Design 9023 temperature chamber and a sample holder (Norwegian Electroceramics) capable of high temperature measurement. The capacitance and dissipation factors of sample were measured at 100 Hz, 1 kHz, 10 kHz, and 100 kHz and temperature varied between 25–450 °C. A heating rate of 3 °C/min was used during measurements.

Samples were prepared for optical analysis by polishing with SiC paper through 1200 grit. Raman spectra were measured using a Renishaw inVia Reflex Raman microscope and 488 nm radiation from a laser excitation source. The laser had an output power of 25 mW and a focused spot size of 200–300 μm through a 5x microscope objective. Raman spectra were measured using a static acquisition centered at 520 cm^{-1} and 15 accumulations with 2 sec exposure times.

III. RESULTS AND DISCUSSION

A. Crystal structure and phase transition studies

Perovskite phase formation, crystal structure, and lattice parameter were determined by XRD at room temperature as a function of x. Figure 2 shows XRD patterns of ceramics in the xPZT-$(1-x)$PNN system with a well crystallized perovskite structure for all compositions. The pyrochlore phase was not observed for any composition in this system. The
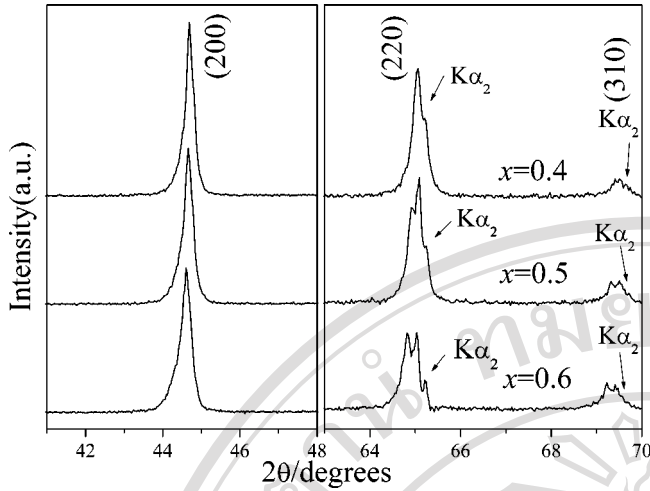
FIG. 3. XRD patterns of the (200) and (220) peaks of xPZT-(1−x)PNN ceramics, x=0.4–0.6.

FIG. 5. Temperature dependence of the relative permittivity ε_r for xPZT-(1−x)PNN ceramics, x=0.4–0.9. Measurement frequencies include 100 Hz, 1 kHz, 10 kHz, and 100 kHz.

crystal symmetry for pure PNN at room temperature is cubic $Pm3m$ with a lattice parameter a=4.031 Å. Below $T_{max} \approx -120$ °C, the symmetry changes to rhombohedral. The crystal structure of $Pb(Zr_{1/2}Ti_{1/2})O_3$ at room temperature is tetragonal. Therefore, with increasing x the crystal symmetry should change due to the effects of the increased PZT fraction and the increase in T_C. Figure 3 shows XRD peak profiles of the (200) and (220) peaks at x=0.4, 0.5, and 0.6. The XRD data shows that the splitting of (200) peak is not observed. At the x=0.4 composition, only a single (220) peak is seen, indicating that the major phase in this composition had cubic symmetry. However, splitting was very clearly observed for the (220) peak in compositions x=0.5 and 0.6, indicating that the crystal transformed into rhombohedral symmetry (pseudocubic). With a further increase in PZT content to x>0.6, the (111) and (200) diffraction peaks begin to split as shown in Fig. 4. Splitting of the (200) peak becomes more pronounced as x approaches 0.9 indicating a stabilization of the tetragonal phase at high PZT concentrations.
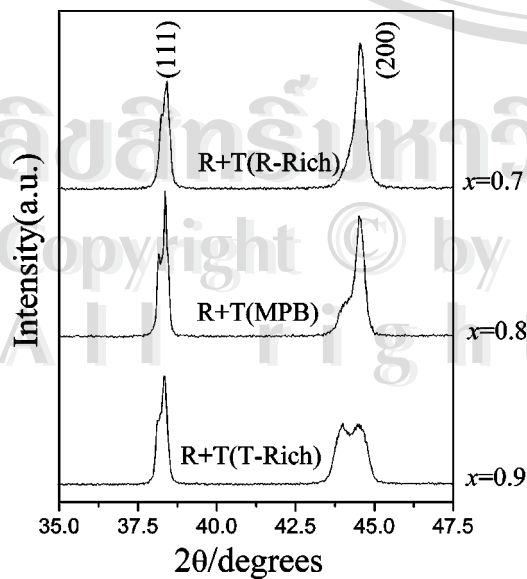

FIG. 4. XRD patterns of the (111) and (200) peaks of xPZT-(1−x)PNN ceramics, x=0.7–0.9.

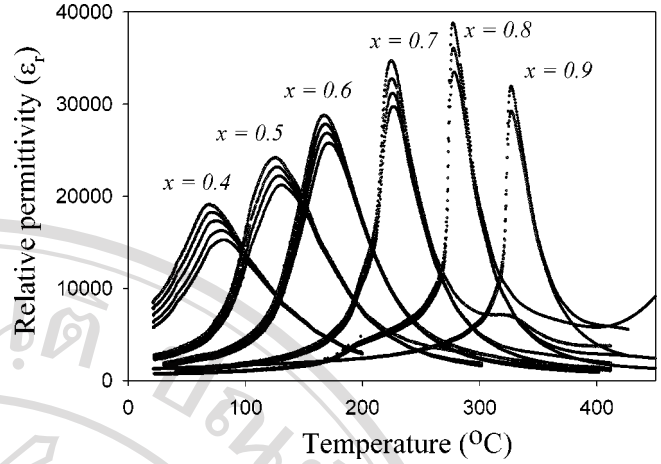At the x=0.8 composition, the unambiguous splitting of (111) peak indicates the coexistence of the rhombohedral and tetragonal phase. Thus there is a transformation from the rhombohedral phase to the tetragonal phase across the compositional range x=0.7–0.9. The x=0.7 composition is within the rhombohedral-rich side of the MPB and the composition x=0.9 is on the tetragonal-rich side of the MPB. It is important to note that recent results have uncovered the existence of a low-symmetry (monoclinic) phase within the MPB region of PZT,[24] $Pb(Mg_{1/3}Nb_{2/3})O_3$-$PbTiO_3$[25] and the orthorhombic phase of $Pb(Zn_{1/3}Nb_{2/3})O_3$-$PbTiO_3$.[26] Given the similarities of PNN-PZT to the $Pb(Mg_{1/3}Nb_{2/3})O_3$-$PbTiO_3$ system, it is possible that a low symmetry monoclinic or orthorhombic phase may be stabilized within the MPB regions of xPZT-(1−x)PNN; x=0.7–0.9.

B. Dielectric properties

The characteristic temperature and frequency dependence of the relative permittivity for xPZT-(1−x)PNN, x=0.4–0.9, is shown in Fig. 5. A clear transition in T_{max} (defined as the temperature at which ε_r is maximum at 10 kHz) is observed with T_{max} increasing with x. At compositions x=0.4, 0.5, and 0.6, the sample displays a pronounced relaxor ferroelectric behavior, characterized by diffuse permittivity peaks and a shift of the maximum permittivity to higher temperatures with increasing frequency. An increase in the magnitude of the maximum permittivity is also observed over this region. The nature of the homogeneously polarized states is believed to be controlled by the concentration of PZT.

A smooth transition from relaxor to normal ferroelectric behavior is observed with increasing mole percent of PZT from x=0.7 to 0.9. This transition is characterized by the enhancement of the first-order nature of the phase transformation and the diminishment of the relaxor behavior (i.e., the permittivity dispersion) over the broad temperature range in the vicinity of T_{max}. From these data, the relaxor-normal transformation is very clearly observed with increased PZT concentration above x=0.7. Furthermore, the relative permittivity and T_{max} increased with increased mole percent of PZT
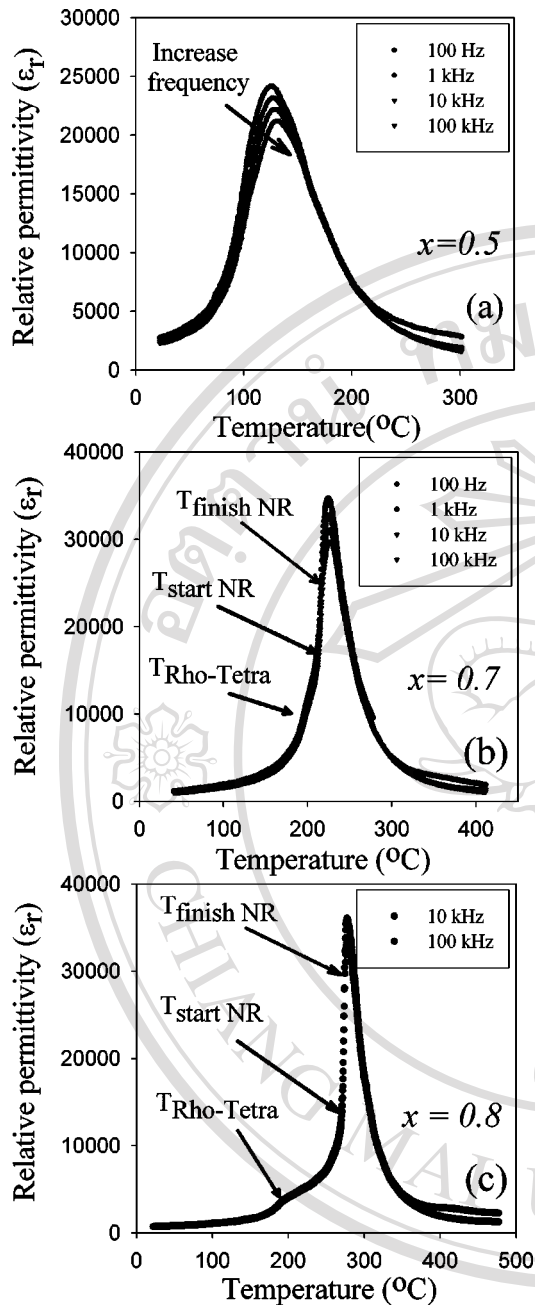
FIG. 6. Temperature dependence of the relative permittivity ε_r for xPZT-$(1-x)$PNN ceramics, A:x=0.5, B:x=0.7, and C:x=0.8.

considerably up to a maximum permittivity at x=0.8. The sharp permittivity peak exhibits a maximum value of 36 000 at 10 kHz for this composition. Figure 6 shows a comparison of the permittivity as a function of temperature for the compositions x=0.5, 0.7, and 0.8 taken over the measurement frequencies of 100 Hz–100 kHz.

For x=0.5, T_{max} increases from 125.6 °C at 100 Hz to 130.8 °C at 100 kHz (ΔT=5.2 °C). The relative permittivity at room temperature was 2830 at 100 Hz and increased to 24 200 at 1 kHz at T_{max} and the maximum value of the relative permittivity decreased with increasing frequency. The dielectric dispersion below T_{max} indicates typical relaxor ferroelectric behavior arising from the responses of polar microdomains within the spectrum of the relaxation

time. For x=0.7 and 0.8 compositions, it is evident that two phase transitions are observed. Over the temperature range 190 to 200 °C, a rhombohedral to tetragonal phase transition is observed for both compositions (indicated in the figure by $T_{\text{Rho-Tetra}}$). Another transition between the ferroelectric tetragonal to paraelectric cubic phase occurs in the temperature ranges 225 °C and 277 °C for x=0.7 and x=0.8, respectively. Although the transition from ferroelectric rhombohedral to tetragonal phase is obscured in the composition x=0.7 it is more clearly evident in the composition x=0.8. Similar phenomena has been observed in single crystal Pb(Zn$_{1/3}$Nb$_{2/3}$)O$_3$-PbTiO$_3$,[11] Pb(In$_{1/2}$Nb$_{1/2}$)O$_3$-PbTiO$_3$,[27] and Pb(Mg$_{1/3}$Nb$_{2/3}$)O$_3$-PbTiO$_3$.[9]

In addition, the transformation from the relaxor ferroelectric state to the normal ferroelectric state can be observed in the composition x=0.7–0.9 as shown in Figs. 5, 6(b), and 6(c). The permittivity sharply increased near the temperature indicated as $T_{\text{start NR}}$ in Figs. 6(b) and 6(c). The subscript "start NR" denotes the initial transition from a normal ferroelectric state to a pure relaxor ferroelectric state. Relaxor behavior was observed at temperatures above $T_{\text{finish NR}}$. The subscript "finish NR" denotes the completion of the transformation. For x=0.7 at temperatures below 212 °C, the relative permittivity did not show any significant dispersion until 218 °C. Above this temperature, the relative permittivity shows a strong frequency dependence. This indicates that at 212 °C 0.7PZT-0.3PNN started to transform a normal ferroelectric state to relaxor ferroelectric state; finishing the transformation at 218 °C. The differential between $T_{\text{start NR}}$ and $T_{\text{finish NR}}$ was approximately 6 °C, 5 °C, and 4 °C for x =0.7, 0.8, and 0.9 respectively. This behavior can be explained by decreasing relaxor stability with increasing x.

At the composition x=0.9, a broad permittivity was observed with a slight frequency dispersion close to T_{max}. A first-order transition response was observed at temperatures slightly below T_{max}. This phenomenon indicates that the polar moments are static, since the polar moments are relatively large. The crystal structure and dielectric properties for all compositions are listed in Table I.

The maximum permittivity $\varepsilon_{r,\text{max}}$ and T_{max} as a function of the mole fraction of PZT(x) are represented in Fig. 7. There is a good linear relationship between T_{max} and x, indicating that this system is a well behaved complete solid solution. The T_{max} of the constituent compounds PNN and PZT are −120 °C and 390 °C, respectively, which can be used to calculate an empirical estimate of T_{max} via the equation,

$$T_{\text{max}} = x(390 \ ^\circ\text{C}) + (1-x)(-120 \ ^\circ\text{C}) \tag{1}$$

The variation of the measured T_{max}, the calculated T_{max}, and the measured $\varepsilon_{r,\text{max}}$ as a function of composition x is shown in Fig. 7. The highest $\varepsilon_{r,\text{max}}$ of 36 000 at 277 °C at 10 kHz was observed for the composition at the MPB 0.8PZT-0.2PNN. It is evident from the data that Eq. (1) gives a reasonable approximation of the transition temperature T_{max}. This result suggests that the transition temperature of xPZT-$(1-x)$PNN system can be varied over a wide range from −120 to 390 °C by controlling the amount of PZT in the system.

TABLE I. Ferroelectric properties of xPZT-$(1-x)$PNN ceramics (C, cubic; R, rhombohedral; T, tetragonal).

Composition x	Crystal structure	T_m(°C) at 10 kHz	Relative permittivity at 25 °C	Relative permittivity at T_{max}	tan δ at 25 °C	tan δ at T_m	δ_γ
x=0.4	C	75.4	7500	17 500	0.062	0.036	29.5
x=0.5	R	128.9	2500	22 000	0.042	0.024	24.4
x=0.6	R	169.7	1600	27 000	0.042	0.018	22.4
x=0.7	R-rich	225.5	1060	31 200	0.029	0.025	14.0
x=0.8	R+T	277.4	835	36 000	0.011	0.047	10.2
x=0.9	T-rich	326.7	950	32 000	0.005	0.182	8.6

It is well known that the permittivity of a first-order normal ferroelectric can be described by the Curie-Weiss law:

$$\frac{1}{\varepsilon_r} = \frac{T - \theta}{C}, \tag{2}$$

where θ is the Curie-Weiss temperature and C is Curie constant. A second-order relaxor ferroelectric can be described by a simple quadratic law. This arises from the fact that the total number of relaxors contributing to the permittivity response in the vicinity of the permittivity peak is temperature dependent, and the temperature distribution of this number is given by a Gaussian function about a mean value T_o with a standard deviation δ. The relative permittivity can be derived via the following expression:[28,29]

$$\frac{\varepsilon_m'}{\varepsilon'(f,T)} = 1 + \frac{[T - T_m(f)]^\gamma}{2\delta_\gamma^2} \ (1 \leqslant \gamma \leqslant 2), \tag{3}$$

where ε_m' is the maximum value of the permittivity at $T = T_m(f)$. The value of γ is the expression of the degree of dielectric relaxation in the relaxor ferroelectric material. When $\gamma=1$ Eq. (3) expresses Curie-Weiss behavior, while for $\gamma=2$ this equation is identical to the quadratic relationship. Many relaxor ferroelectric materials can be fit to Eq. (3) with $\gamma=2$ at temperatures above T_{max}. The parameter δ_γ can be used to measure the degree of diffuseness of the phase transition in mixed relaxor-normal ferroelectric materials. The values γ and δ_γ are both material constants depending on the composition and structure of the material. The δ_γ

value can be determined from the slope of $\varepsilon_m'/\varepsilon'$ versus $(T -T_m)^2$, which should be linear.

The δ_γ values of compositions in the xPZT-$(1-x)$PNN system are represented in Fig. 8. Both the diffuseness parameter δ_γ and γ decreased with an increase in the mole fraction of PZT. As illustrated in Fig. 9, a near linear relationship was observed over the wide compositional range, which is consistent with a perfect solid solution. The diffuseness of the phase transition in the x=0.4 composition can be attributed to the relaxor nature of PNN. As the PZT content increased, the relaxor characteristic of xPZT-$(1-x)$PNN was observed to decrease. This is because the substitution of $(Zr_{1/2}Ti_{1/2})^{4+}$ for the B-site complex ions $(Ni_{1/3}Nb_{2/3})^{4+}$ increases the size of the local polar domains by strengthening the off-center displacement and enhancing the interactions between micropolar domains. As was observed in $Pb(Mg_{1/3}Nb_{2/3})O_3$-$PbTiO_3$ crystals,[30] this leads to the formation of macropolar domains which break the symmetry of the pseudocubic state.
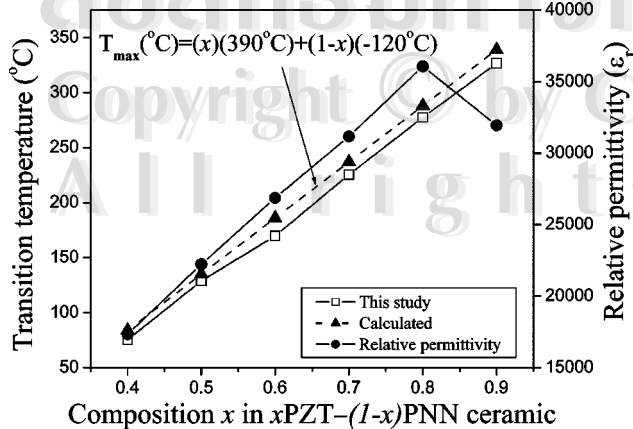

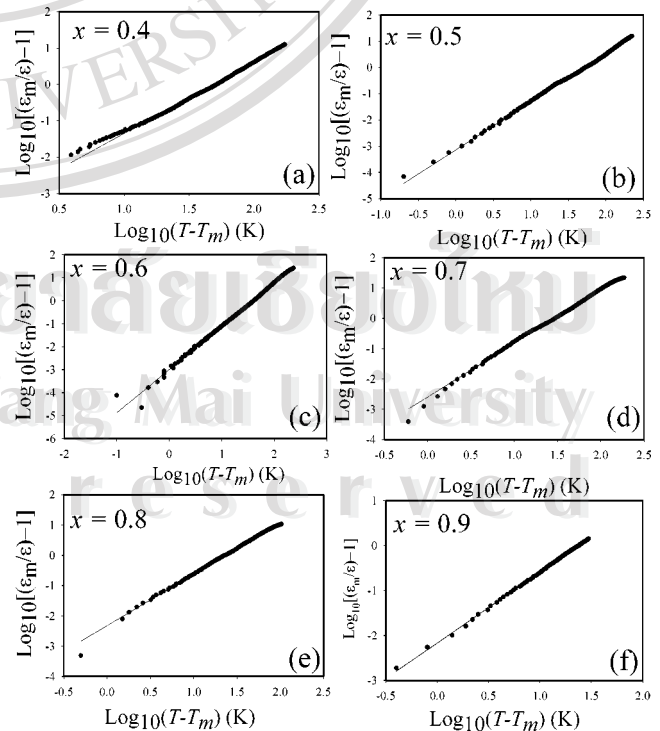FIG. 7. T_{max}, calculated T_{max}, and maximum ε_r as a function of composition x at 10 kHz.

FIG. 8. $Log_{10}[(\varepsilon_m/\varepsilon)-1]$ vs $Log_{10}(T-T_{max})$ for xPZT-$(1-x)$PNN ceramics, x=0.4–0.9.
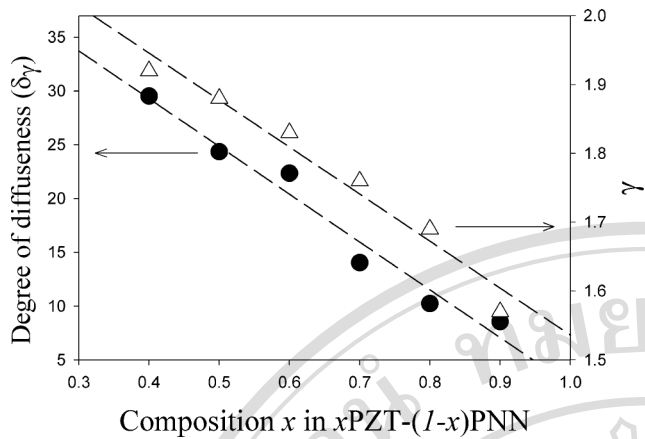
FIG. 9. Parameter γ and degree of diffuseness (δ_γ) vs x for xPZT-$(1-x)$PNN ceramics, $x=0.4–0.9$.

C. Raman spectroscopy of $Pb(Zr_{1/2}Ti_{1/2})O_3$-$Pb(Ni_{1/3}Nb_{2/3})O_3$

Figure 10 shows the Raman spectra of ceramic xPZT -$(1-x)$PNN with $x=0.4$ to 0.9. The individual spectral data was analyzed using Bruker Optics OPUS software. A multi-peak pattern was fit to the data using Lorentz-Gauss peak shape parameters and Levenberg-Marquardt refinement techniques. The resulting peak locations for each xPZT-$(1-x)$PNN sample is shown in Fig. 11. Each peak represents a Raman active vibration mode frequency for the given composition. Peak location and intensity will vary depending on the type of bonds present in the material. There is a distinct difference in pattern when going from $x=0.4–0.5$. The disappearance of modes at 440 and 560 cm^{-1} and the appear-
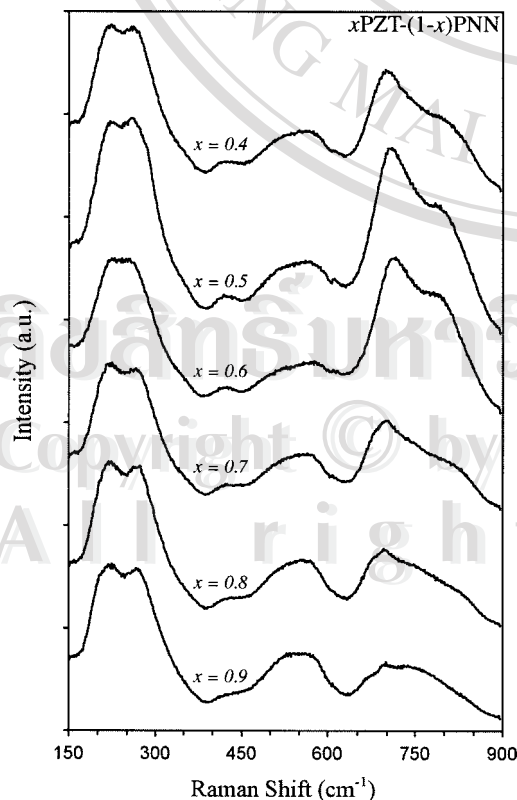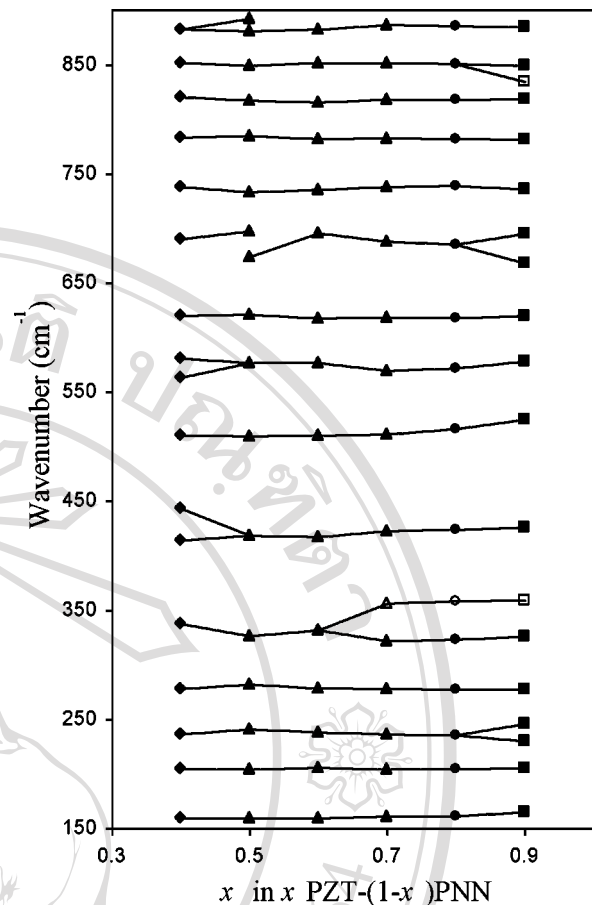

FIG. 11. Wave number as a function of composition x for ceramic xPZT-$(1-x)$PNN with $x=0.4$ to 0.9.

ance of modes at 675 and 890 cm^{-1} are indicative of a change in phase. The same is indicated for $x=0.7–0.8$, where a weak mode at 350 cm^{-1} first appears at $x=0.7$ and gains intensity for $x=0.8–0.9$. There is yet another change in mode pattern when going from $x=0.8–0.9$, where modes appear at 250, 670, and 834 cm^{-1}. These modes represent the splitting of a single mode for $x=0.8$.

D. Phase diagram of $Pb(Zr_{1/2}Ti_{1/2})O_3$-$Pb(Ni_{1/3}Nb_{2/3})O_3$

Based on the results of x-ray diffraction, dielectric spectroscopy, and Raman spectroscopy, the phase diagram for the xPZT-$(1-x)$PNN binary system have been established as shown in Fig. 12. The transition temperature increases approximately linearly with x, from $T_{max}=75\ °C$ for $x=0.4$ to 340 °C for $x=0.9$. The phase diagram consists of four distinct crystallographic phases in this system; high temperature paraelectric cubic ($Pm3m$), pseudocubic relaxor, rhombohedral relaxor ($R3m$), and normal ferroelectric tetragonal ($P4mm$). At low concentrations of PZT $x \leqslant 0.4$ the symmetry can be defined as pseudocubic. The pseudocubic symmetry transforms into rhombohedral at the composition near $x=0.5$. The ferroelectric rhombohedral and tetragonal phases are separated by an MPB region which is located near the composition $x=0.8$ below 277 °C. Within this region, both the rhombohedral and tetragonal phases coexist. In most perovskite systems, the width of the MPB is limited though there may be low symmetry phases present.[24–26] In this work,
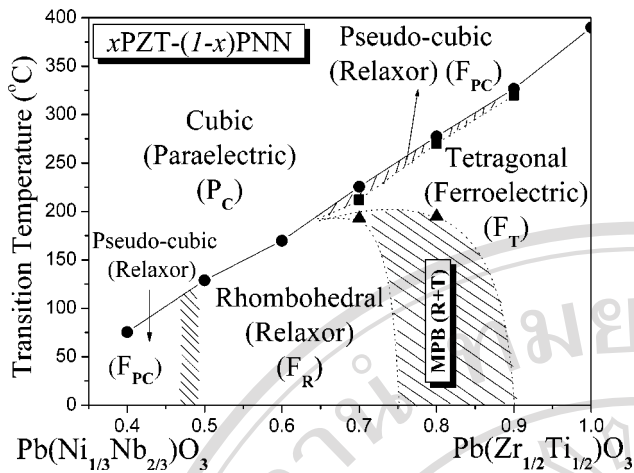

FIG. 10. Raman spectra of ceramic xPZT-$(1-x)$PNN with $x=0.4$ to 0.9.

FIG. 12. Phase diagram of xPZT-$(1-x)$PNN, $x=0.4-0.9$ quasibinary system.

Fig. 12 shows the MPB region as broad because of the limited number of compositions in this study. Also, due to the nature of the ceramic preparation technique, mixed phases may be present within the MPB due to local compositional variations. Future work will be focused on identifying the width of the MPB and establishing the phase equilibria in the vicinity of the MPB.

IV. CONCLUSIONS

In this work the ferroelectric properties of the solid solution between relaxor ferroelectric PNN and normal ferroelectric PZT(50/50) have been investigated. The crystal structure data obtained from XRD indicates that the solid solution xPZT-$(1-x)$PNN, where $x=0.4-0.9$, successively transforms from pseudocubic to rhombohedral to tetragonal symmetry with an increase in PZT concentration. The XRD results were reinforced by Raman spectral analysis. The new MPB in this binary system is located near $x=0.8$, separating the rhombohedral and tetragonal phases. At the MPB composition, the permittivity exhibited a shoulder at T_{RT} $=195\ ^{\circ}$C indicating a rhombohedral to tetragonal phase transformation with a maximum permittivity of 36 000 at 10 kHz at $T_{max}=277\ ^{\circ}$C. Moreover a transition from relaxor to normal ferroelectric behavior is clearly observed above a PZT concentration $x=0.7$. Furthermore, this transition be-

tween relaxor to normal ferroelectricity was typified by a quasilinear relationship between the diffuseness parameter δ_{γ} and PZT mole fraction x.

[1] G. A. Smolenskii and A. L. Agranovskaya, Sov. Phys. Tech. Phys. **2**, 1380 (1958).
[2] V. A. Bokov and I. E. Myl'nikova, Sov. Phys. Solid State **3**, 613 (1961).
[3] C. A. Randall and A. S. Bhalla, Jpn. J. Appl. Phys., Part 1 **29**, 327 (1990).
[4] V. A. Bokov and I. E. Mylnikova, Sov. Phys. Solid State **2**, 2428 (1960).
[5] K. Uchino, *Ferroelectric Devices* (Marcel Dekker, New York, 2000).
[6] A. J. Moulson and J. M. Herbert, *Electroceramics Materials, Properties: Appications* (Chapman and Hall, New York, 1990).
[7] K. Uchino, Solid State Ionics **108**, 43 (1998).
[8] S. -E. Park and T. R. Shrout, IEEE Trans. Ultrason. Ferroelectr. Freq. Control **44**, 1140 (1997).
[9] T. R. Shrout, Z. P. Chang, N. Kim, and S. Markgraf, Ferroelectr., Lett. Sect. **12**, 63 (1990).
[10] J. Kuwata, K. Uchino, and S. Nomura, Ferroelectrics **37**, 579 (1981).
[11] M. L. Mulvihill, L. E. Cross, W. Cao, and K. Uchino, J. Am. Ceram. Soc. **80**, 1462 (1997).
[12] H. Ouchi, K. Nagano, and S. Hayakawa, J. Am. Ceram. Soc. **48**, T26–T31 (1965).
[13] H. Fan and H. E. Kim, J. Mater. Res. **17**, 180 (2002).
[14] Y. Yamashita, Jpn. J. Appl. Phys., Part 1 **33**, 4652 (1994).
[15] V. J. Tennery, K. W. Hang, and R. E. Novak, J. Am. Ceram. Soc. **51**, 671 (1968).
[16] D. Luff, R. Lane, K. R. Brown, and H. J. Marshallsay, Trans. J. Br. Ceram. Soc. **73**, 251 (1974).
[17] E. A. Buyanova, P. L. Strelets, I. A. Serova, and V. A. Isupov, Bull. Acad. Sci. USSR, Phys. Ser. (Engl. Transl.) **29**, 1877 (1965).
[18] G. Robert, M. Demartin, and D. Damjanovic, J. Am. Ceram. Soc. **81**, 749 (1998).
[19] E. F. Alberta and A. S. Bhalla, Int. J. Inorg. Mater. **3**, 987 (2001).
[20] O. Babushkin, T. Lindback, J. C. Luc, and J. Y. M. Leblais, J. Eur. Ceram. Soc. **18**, 737 (1998).
[21] G. Robert, M. D. Maeder, D. Damjanovic, and N. Setter, J. Am. Ceram. Soc. **84**, 2869 (2001).
[22] Z. Li and X. Yao, J. Mater. Sci. Lett. **20**, 273 (2001).
[23] M.-S. Yoon and H. M. Jang, J. Appl. Phys. **77**, 3991 (1995).
[24] B. Noheda, D. E. Cox, G. Shirane, J. A. Gonzalo, L. E. Cross, and S.-E. Park, Appl. Phys. Lett. **74**, 2059 (1999).
[25] Z.-G. Ye, B. Noheda, M. Dong, D. Cox, and G. Shirane, Phys. Rev. B **64**, 184114 (2001).
[26] D. La-Orauttapong, B. Noheda, Z.-G. Ye, P. M. Gehring, J. Toulouse, D. E. Cox, and G. Shirane, Phys. Rev. B **65**, 144101 (2002).
[27] Y. Guo, H. Luo, and T. He, Mater. Res. Bull. **38**, 85 (2003).
[28] H. T. Martirena and J. C. Burfoot, Ferroelectrics **7**, 151 (1974).
[29] K. Uchino and S. Nomura, Ferroelectr., Lett. Sect. **44**, 55 (1982).
[30] Z.-G. Ye and M. Dong, J. Appl. Phys. **87**, 2312 (2000).

Influence of Processing Conditions on the Morphotropic Phase Boundaries and Ferroelectric Properties of $Pb(Zn_{1/3}Nb_{2/3})O_3$-$Pb(Ni_{1/3}Nb_{2/3})O_3$-$Pb(Zr_{1/2}Ti_{1/2})O_3$ Solid Solutions

David P. Cann, Xiaoli Tan
Materials Science and Engineering
Iowa State University
Ames, IA 50011 USA
BaTiO3@iastate.edu

Naratip Vittayakorn, Gobwute Rujijanagul, and
Tawee Tunkasiri
Department of Physics, Faculty of Science
Chiang Mai University
Chiang Mai, 50200 Thailand

Abstract— **Ceramic solid solutions within the ternary system of $Pb(Zn_{1/3}Nb_{2/3})O_3$ - $Pb(Ni_{1/3}Nb_{2/3})O_3$ - $Pb(Zr_{1/2}Ti_{1/2})O_3$ (PZN-PNN-PZT) were synthesized via two methods: the mixed oxide method and the columbite method. Phase development of the calcined powders and the crystal structure of sintered ceramics were analyzed by x-ray diffraction. The ferroelectric properties of the ceramics were characterized by a combination of dielectric and hysteresis measurements. It was observed that for the binary systems PZN-PZT and PNN-PZT, the change in the transition temperature (T_m) is nearly linear with respect to the PZT content. Ferroelectric properties were analyzed to elucidate the nature of the phase transformation and identify the impact of the processing conditions. With these data, ferroelectric phase diagrams were derived showing the transition between the pseudo-cubic relaxor behavior of PZN and PNN to the tetragonal normal ferroelectric behavior of PZT. This transition was also correlated to changes in the diffuseness parameter δ_γ. When comparing ceramics prepared by the columbite method and the mixed oxide route, ceramics prepared by the mixed oxide method showed a lower remanent polarization P_r and a higher coercive field E_c. Additionally, ceramics prepared by the columbite method displayed sharp transitions in ferroelectric properties across the MPB composition, whereas these transitions were obscured in ceramics prepared by the mixed oxide method. It is proposed that the different reaction paths influenced the degree of compositional heterogeneity in these complex perovskite solid solutions, which was clearly reflected in the nature of the phase transition.**

Keywords: morpotropic phase boundary, columbite method, perovskite, phase transition

I. INTRODUCTION

Ferroelectric materials based on Pb-perovskites have found use in countless applications including piezoelectric sensors and actuators, capacitors, pyroelectric and electro-optic devices, and ferroelectric memories [1,2]. In many instances, compositions near a morphotropic phase boundary (MPB) between ferroelectric phases of different symmetry have advantageous dielectric and piezoelectric performance

characteristics [1,3]. There have been a number of MPB's identified in Pb-based systems including the most widely exploited system $PbZrO_3$-$PbTiO_3$ (PZT) [3]. Other MPB systems include $Pb(Mg_{1/3}Nb_{2/3})O_3$-$PbTiO_3$ (PMN-PT) [4], $Pb(Zn_{1/3}Nb_{2/3})O_3$-$PbTiO_3$ (PZN-PT) [5], $Pb(Sc_{1/2}Nb_{1/2})O_3$-$PbTiO_3$ (PSN-PT) [6], and many others.

This work will focus on perovskite solid solutions in two quasi-binary systems within the overall ternary system $Pb(Zr_{1/2}Ti_{1/2})O_3$- $Pb(Zn_{1/3}Nb_{2/3})O_3$- $Pb(Ni_{1/3}Nb_{2/3})O_3$: specifically $Pb(Zn_{1/3}Nb_{2/3})O_3$-$Pb(Zr_{1/2}Ti_{1/2})O_3$ (PZN-PZT) and $Pb(Ni_{1/3}Nb_{2/3})O_3$-$Pb(Zr_{1/2}Ti_{1/2})O_3$ (PNN-PZT). Polycrystalline ceramics based on Pb-perovskites are typically synthesized through high temperature solid state processes. A number of processing methods have been proposed to ensure phase pure perovskite. In this work, two common processing methods will be contrasted with the aim of understanding the influence of processing conditions on the phase equilibria and ferroelectric properties. The conventional mixed oxide method involves simply reacting all of the binary oxides (e.g. PbO, TiO_2, ZrO_2, etc.) in a single calcination step to form the desired perovskite phase. In the columbite method, first proposed by Swartz and Shrout [7], the B-site oxides are first pre-reacted to form intermediate phases such as $ZnNb_2O_6$, $ZrTiO_4$, $NiNb_2O_6$, etc. These intermediate phases are then reacted with PbO to form the desired perovskite phase.

Given that the PZN-PNN-PZT phases are all perovskite solid solutions, it is likely that the different reaction paths may lead to distinct differences in the homogeneity of the B-cation distributions. In this study, a combination of x-ray diffraction (XRD), dielectric measurements, and Raman spectroscopy will be employed to probe the influence of the different processing methods on such parameters as the perovskite phase distributions, remanent polarization (P_r), coercive field (E_C), diffuseness parameter (δ_γ), and others. With this information, it will be possible to optimize the processing conditions for solid solutions near MPBs.

II. EXPERIMENTAL

The columbite precursors $ZnNb_2O_6$ and $NiNb_2O_6$ were prepared from the reaction between ZnO (99.9%) and Nb_2O_5 (99.9%) at 975^oC for 4h and between NiO (99.9%) and Nb_2O_5 (99.9%) for 4h at 1100^oC, respectively. The wolframite phase $ZrTiO_4$ was formed by reacting ZrO_2 (99.9%) with TiO_2(99.9%) at 1400^oC for 4h. The powders of $ZnNb_2O_6$, $NiNb_2O_6$, and $ZrTiO_4$ were mixed in the required stoichiometric amounts with PbO (99.9%) with an excess of 2 mol% of PbO added. The milling process was carried out for 24 hours in isopropyl alcohol. The powders were calcined at 900^oC-950^oC for 4 h in a double crucible configuration with a heating rate of 20^oC/min. After grinding and sieving, 5 wt% of polyvinyl alcohol (PVA) binder was added. Discs with a diameter of 12.5 mm were prepared by cold uniaxial pressing at a pressure of 150MPa. Binder burnout occurred by slow heating to 500^oC and holding for 2h. The discs were sintered in a sealed alumina crucible at temperatures ranging from 950^oC-1250^oC using a heating rate of 5^oC/min and a dwell time of 2 h. To prevent PbO volatilization from the discs, a PbO atmosphere was maintained by placing a bed of $PbZrO_3$ powder in the crucible.

Phase formation and crystal structure of the calcined powders and sintered discs were examined by x-ray diffraction (XRD). The pellets were polished and electroded via gold sputtering, over which a layer of air-dried silver paint was applied. The relative permittivity (ε') and dissipation factor (tan δ) of the pellets sample were measured at various temperatures over the frequency range between 100 and 100KHz using an LCR meter (HP 4284A). The remanent polarization P_r was determined from a P-E hysteresis loop measurements using a Sawyer-Tower circuit at temperatures between -66^oC and 60^oC.

III. RESULTS

Single phase perovskite was obtained for the pseudo-binary systems over the composition ranges *(1-x)*PZN-*x*PZT at $0.5 \leq x \leq 0.9$ and for *(1-x)*PNN-*x*PZT at $0.4 \leq x \leq 0.9$. For the 0.6PZN-0.4PZT composition a small amount of pyrochlore phase was noted. The results of the XRD, dielectric, and Raman measurements and the influence that can be attributed to processing conditions are summarized for each pseudo-binary system in the following sections.

A. PZN-PZT System

In the PZN-PZT system, phase pure perovskite was obtained at lower calcination temperatures using the conventional method compared to the columbite method. As shown in Fig. 1, the columbite method required calcination temperatures as much as 150°C higher for some PZN-PZT compositions. This effect was especially prevalent at high mole fractions of PZT. In analyzing the phase evolution at low temperatures, a high volume fraction of a pyrochlore phase was observed in the XRD data for the columbite derived powders. In the conventionally prepared powders the perovskite phase was the dominant phase even at 750°C. This suggests that each processing route followed a different reaction path in eventually forming the perovskite phase.
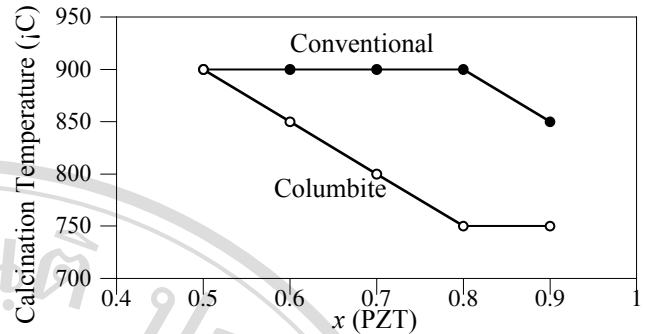

Figure 1. Calcination temperature at which phase pure perovskite is obtained for both the conventional and columbite methods.

The symmetry of the resultant perovskite phases obtained through XRD allows a pseudo-binary phase diagram to be derived (Fig. 2). Compositions close to PZT are tetragonal at room temperature, with a transition to rhombohedral symmetry for compositions at $x \leq 0.7$. Inspection of the XRD patterns of compositions close to the MPB at $x \approx 0.7$ revealed that the processing method had an influence on the phase distribution (Fig. 3). In columbite derived powders, only the rhombohedral perovskite phase was observed. However, in conventionally prepared powders a mixture of the rhombohedral and tetragonal phases were observed. This is strong evidence that the conventional method produces non-uniform mixing of the B-site cations as compared to the columbite method.
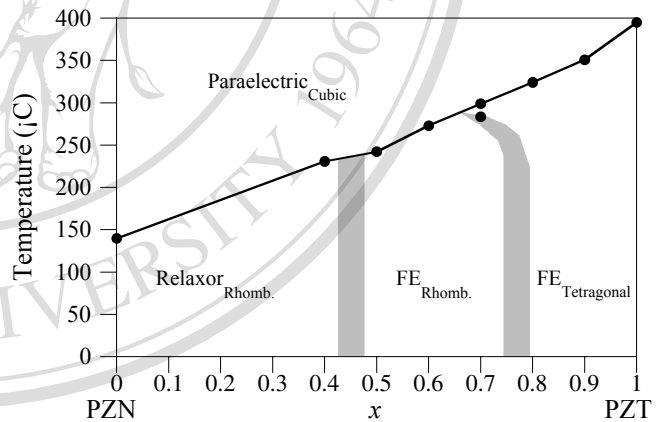

Figure 2. PZN-PZT phase diagram obtained through room temperature XRD and dielectric measurements.

Further evidence is seen in the dielectric data presented in Fig. 4. For compositions near the MPB at $x = 0.7$, a phase transition was clearly seen in the columbite derived ceramics at 284°C. As indicated in the phase diagram (Fig. 2), this corresponds to a transition from rhombohedral to tetragonal symmetry. The conventionally prepared ceramics at $x = 0.7$ did not show any anomalies within that temperature range.

Comparisons of the dielectric data for PZN-PZT ceramics prepared by the two methods are presented in Table I. These data show that ceramics prepared via the columbite method exhibit a significantly higher room temperature permittivity, higher permittivity at T_{max}, and a higher remanent polarization (P_r) determined from hysteresis measurements.
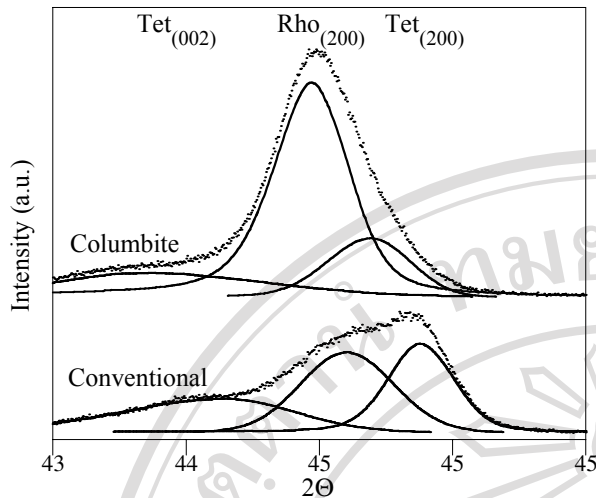
Figure 3.   XRD patterns for the (002) peak for conventional and columbite prepared ceramics. Deconvolution of the data shows that relative proportions of the rhombohedral and tetragonal phases.
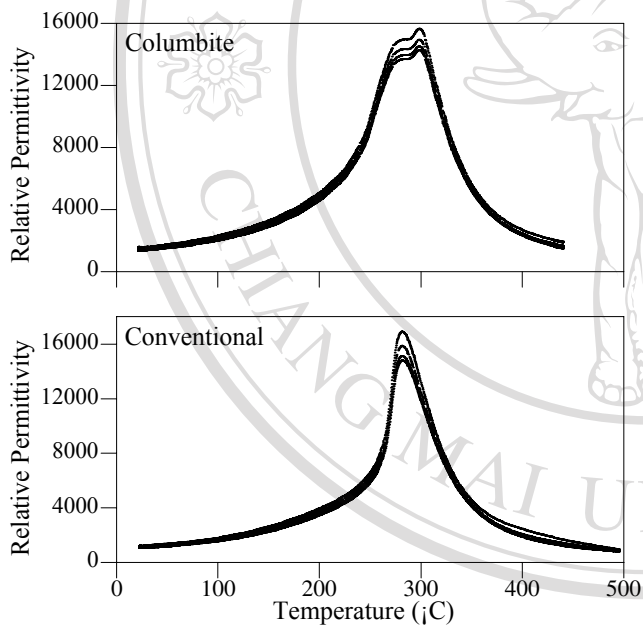

Figure 4.   Relative permittivity versus temperature for a 0.3PZN-0.7PZT ceramic at measurement frequencies of 0.1, 1, 10, and 100 KHz.

x	K at 25°C		K at T_{max}		P_r	
	Conv.	Col.	Conv.	Col.	Conv.	Col.
0.4	1,230	1,440	11,400	13,200		
0.5	1,220	1,430	20,800	21,200	29.5	36.4
0.6	1,230	1,440	17,000	20,800	23.2	30.6
0.7	980	1,580	14,300	15,700	20.0	30.4
0.8	1,230	1,550	25,000	25,800	31.5	36.1
0.9	810	1,590	13,300	21,200	34.0	37.1

Taking all of these results into account, PZN-PZT ceramics prepared by the columbite method exhibited more clearly defined phase transitions and MPBs compared to conventionally processed ceramics. Rhombohedral distortions in perovskites are linked to the geometric tolerance factor (*t*). In the PZN-PZT system, the magnitude of *t* is determined by the average B-cation radius. In the conventionally prepared ceramics, the coexistence of the tetragonal and rhombohedral phases near the MPB are indicative of a significant degree of variation in the composition of the B-site. Regions which were rich in smaller cations would favor tetragonal distortions, whereas regions rich in larger cations would favor rhombohedral distortions.   The formation of columbite oxides prior to perovskite formation assures intimate mixing of the B-site cations.   This ultimately leads to a more homogeneous distribution of B-site cations.
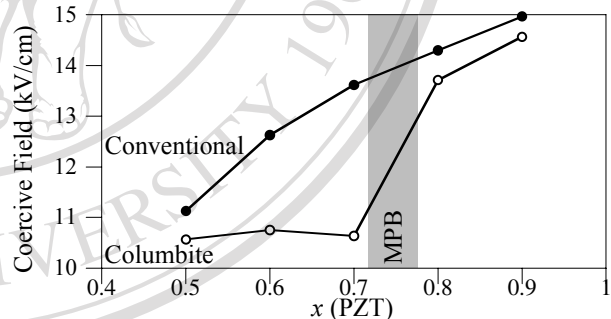

Figure 5.   Coercive field as a function of composition *x* for columbite and conventionally prepared ceramics.

It is important to note that there were no significant differences in the density or grain size when comparing the two processing methods. All samples in this study were of high density ($\rho_{Theoretical} > 96\%$) with grain sizes close to 5 μm. Therefore, it is possible to exclude the influence of density or grain size effects from these results.

In Fig. 5, the coercive field (E_C) as a function of *x* exhibits very different trends comparing the conventional and columbite prepared ceramics. The columbite ceramics exhibited a sharp transition in E_C at the MPB, whereas the conventionally prepared ceramic displayed a gradual transition.

B.   PNN-PZT System

In the PNN-PZT system, the columbite method was utilized to prepare phase-pure perovskite ceramics. Based on room temperature XRD and measurements of the relative permittivity versus temperature a phase diagram for PNN-PZT was derived (Fig. 6). At *x* = 0.8, an MPB region separates a tetragonal normal ferroelectric phase field from a rhombohedral relaxor ferroelectric phase field. XRD data within the MPB region featured splitting of both (200) and (111) peaks. This is indicative of the coexistence of both rhombohedral and tetragonal phases. Alternatively, as has been demonstrated in PZT the multiple peak splitting could be indicative of another lower symmetry phase (e.g. monoclinic) [8].
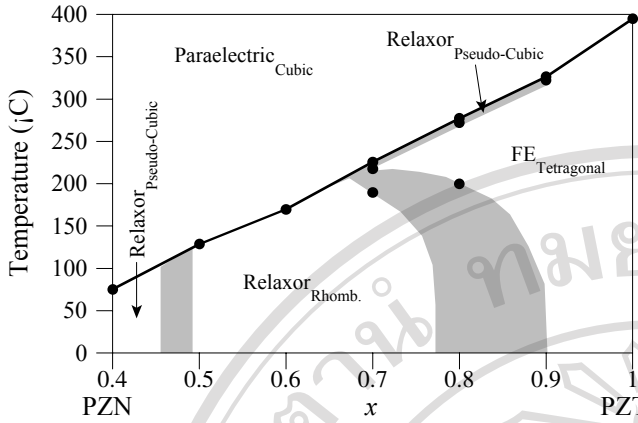
Figure 6. PNN-PZT phase diagram obtained through room temperature XRD and dielectric measurements.

Table II summarizes the results of the dielectric measurements on the PNN-PZT ceramics. As expected, the relative permittivity peaked at the MPB composition ($x = 0.8$) at a value of 36,000. A general transition from normal ferroelectric to relaxor ferroelectric behavior was observed as the mole fraction of PNN increased. Fig. 7 illustrates the relative permittivity versus temperature for $0.4 \leq x \leq 0.9$. The transition from normal ferroelectric behavior to relaxor ferroelectric behavior was clearly observed from the dispersion in the vicinity of T_{max}.
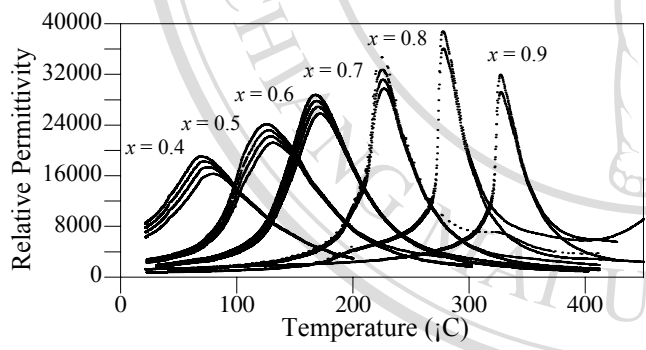

Figure 7. Relative permittivity versus temperature for $(1-x)$PNN-xPZT ceramics.

TABLE II. PNN-PZT DIELECTRIC DATA

x	T_{max} (°C)	K at 25°C	tan δ at 25°C	K at T_{max}	δ_γ
0.4	75.4	7,500	0.062	17,500	29.5
0.5	128.9	2,500	0.042	22,000	24.4
0.6	169.7	1,600	0.042	27,000	22.4
0.7	225.5	1,060	0.029	31,200	14.0
0.8	277.4	835	0.011	36,000	10.2
0.9	326.7	950	0.005	32,000	8.6

The parameter δ_γ can be used to quantify the diffuseness of the ferroelectric transition through the equation [9]:

$$\frac{K_{max}}{K(f,T)} = 1 + \frac{\left[T - T_{max}(f)\right]^\gamma}{2\delta_\gamma^2} \tag{1}$$

where $\gamma = 1$ for Curie-Weiss behavior and $\gamma = 2$ for pure relaxor character. As shown in Table II, the δ_γ parameter increased linearly with increased PNN content.

IV. CONCLUSIONS

In this work, the ferroelectric phases within the pseudo-binary systems PZN-PZT and PNN-PZT were characterized. For the PZN-PZT compositions, MPBs were noted at $x \approx 0.75$ and $x \approx 0.45$. It was observed pre-reacting the B-site cations via the columbite method had significant effects on the perovskite phase stability and dielectric properties. These effects were most pronounced in the vicinity of the MPB, located near $x \approx 0.75$. It is likely that the columbite method produced a more homogeneous distribution of the B-site cations compared to the mixed oxide prepared ceramics. These compositional variations could be inferred from the observation of multiple phases near the MPB and poorly defined phase transitions.

In the PNN-PZT compositions, two MPBs were noted at $x \approx 0.8$ and $x \approx 0.45$. Even with columbite prepared ceramics, rhombohedral and tetragonal phases were found to coexist at the MPB at $x \approx 0.8$. It is interesting to note that in PNN the transition from the tetragonal PZT phase to the relaxor rhombohedral phase is more gradual than in PZN. This is likely due to the much closer B-cation radii match between $Zr_{0.5}Ti_{0.5}$ (0.803 Å) and $Ni_{1/3}Nb_{2/3}$ (0.797 Å), as compared to $Zn_{1/3}Nb_{2/3}$ (0.813 Å).

REFERENCES

[1] A. J. Moulson and J. M. Herbert, Electroceramics: Materials, Properties, Applications. New York: Chapman and Hall, 1990.

[2] K. Uchino, Ferroelectric Devices. New York: Marcel Dekker, Inc., 2000.

[3] B. Jaffe and W. R. Cook, Piezoelectric ceramics. R.A.N., 1971.

[4] S. W. Choi, T. R. Shrout, S. J. Jang, and A. S. Bhalla, "Dielectric and pyroelectric properties in the Pb(Mg$_{1/3}$Nb$_{2/3}$)O$_3$-PbTiO$_3$ system," Ferroelectrics, vol. 100, 1989.

[5] J. Kuwata, K. Uchino, and S. Nomura, "Dielectric and piezoelectric properties of 0.91Pn(Zn$_{1/3}$Nb$_{2/3}$)O$_3$-0.09PbTiO$_3$ single crystals.," Jpn. J. Appl. Phys., vol. 21, pp. 1298-1302, 1982.

[6] V. J. Tennery, K. W. Hang, and R.E.Novak, "Ferroelectric and structure properties of Pb(Sc$_{1/2}$Nb$_{1/2}$)$_{1-x}$Ti$_x$O$_3$ system," J. Am. Ceram. Soc., vol. 51, pp. 671-674, 1968.

[7] S. L. Swartz and T. R. Shrout, "Fabrication of perovskite lead magnesium niobate," Mater. Res. Bull., vol. 17, pp. 1245, 1982.

[8] B. Noheda, D.E. Cox, G. Shirane, J.A. Gonzalo, L.E. Cross, and S-E. Park, "A monoclinic ferroelectric phase in the Pb(Zr$_{1-x}$Ti$_x$)O$_3$ solid solution," Appl. Phys. Lett. Vol. 74, pp. 2059 (1999).

[9] K.Uchino and S.Nomura, "Critical exponents of the dielectric constants in diffused phase transition crystals," Ferroelectrics Letters, vol. 44, pp. 55, 1982.

VITA

Name-Surname : NaratipVittayakorn

Date of birth : 10 March 1977

Province : Chiang Mai

Education : M.Sc.(Materials), Chiang Mai university

Chiang Mai (2001)

Scholarship : Ph.D. Scholarship from the Ministry of university affairs of

Thailand

Conference and Publications

National Conference:

1. Preparation 0-3 Carbon/HDPE Composites *"The First Thailand Materials Science and Technology Conference, Bangkok (2000)"* W. Tumajaree , **N. Vittayakorn** , G. Rujijanagul , S. Ananta

2. Effects of carbon on properties of 0-3 PZT/HDPE Composites *"The 27th Congress on Science and Technology of Thailand", Songkla University (2001)* **N.Vittayakorn** , G. Rujijanagul ,Tawee Tunkasiri

3. Effect of Calcined Temperature to Phase Formation of zinc niobate and zirconium titanate*"The 2nd Thailand Materials Science and Technology Conference", Bangkok (2002)* **N.Vittayakorn** , G. Rujijanagul ,Tawee Tunkasiri

International Conference:

1. Properties of 0-3 Carbon/HDPE Composites *"The 2nd Asian Microscopy Conference and 18th Annual conference of EMST", Khon Kaen,Thailand (2001)***N. Vittayakorn** ,W. Tumajaree ,G. Rujijanagul , Tawee Tunkasiri

2. Piezoelectric Properties of 0-3 PZT/HDPE Composites *"The 3nd Asean Microscopy Conference and 19th Annual conference of EMST", Chiang Mai,Thailand (2002)* **N.Vittayakorn** , G. Rujijanagul ,Tawee Tunkasiri

3. Effects of Doping Carbon Technique on Properties of 0-3 PZT/HDPE Composites *"The First International Conference on Materials Processing for Properties and Performance", Singapore (2002)* **N.Vittayakorn** , G. Rujijanagul ,Tawee Tunkasiri

4. Phase Formation, Piezoelectric, and Dielectric Properties of the PNN-PZN-PZT System *"105th Annual Meeting & Exposition of The American Ceramic Society" United State of American (2003)* **N.Vittayakorn** , G. Rujijanagul ,Tawee Tunkasiri

5. Perovskite stabilization, microstructural evolution, and ferroelectric properties of the solid solution $0.5Pb(Ni_{1/3}Nb_{2/3})O_3-(0.5-x)$ $Pb(Zn_{1/3}Nb_{2/3})O_3-xPb(Zr_{1/2}Ti_{1/2})O_3$ *"106th Annual Meeting & Exposition of The American Ceramic Society" United State of American (2004)* **N.Vittayakorn** , G. Rujijanagul ,Tawee Tunkasiri, X. Tan and David P. Cann

6. Influence of Processing Conditions on the Morphotropic Phase Boundaries and Ferroelectric Properties of $Pb(Zn_{1/3}Nb_{2/3})O_3-Pb(Ni_{1/3}Nb_{2/3})O_3-Pb(Zr_{1/2}Ti_{1/2})O_3$ System *"106th Annual Meeting & Exposition of The American Ceramic Society" United State of American (2004)* **N.Vittayakorn** , G. Rujijanagul , M.Marquardt, X. Tan and David P. Cann

7. Influence of Processing Conditions on the Morphotropic Phase Boundaries and Ferroelectric Properties of $Pb(Zn_{1/3}Nb_{2/3})O_3$-$Pb(Ni_{1/3}Nb_{2/3})O_3$-$Pb(Zr_{1/2}Ti_{1/2})O_3$ System *"the14th IEEE international symposium on Applications of Ferroelectric (ISAF)"Canada (2004)* David P. Cann, G. Rujijanagul , M.Marquardt, X. Tan and **N.Vittayakorn**

8. Synthesis and characterization solid solution PZN-PZT ceramics. *"The international conference on smart materials smart/intelligent materials and nanotechnology"* Thailand (2004) **N.Vittayakorn** , G. Rujijanagul, X. Tan and David P. Cann

9. Piezoelectric properties of $(1-x)Pb(Zr_{1/2}Ti_{1/2})O_3$-$xPb(Zn_{1/3}Nb_{2/3})O_3$ ceramics prepared by the columbite-(wolframite) precursor method. *"2nd International Conference on Advanced Materials and Nanotechnology (AMN-2)"* New Zealand (2005) **N. Vittayakorn**, G. Rujijanagul, X. Tan and D. P. Cann

International Publications

1. **N. Vittayakorn**, G. Rujijanagul, T. Tunkasiri, X. Tan and D. P. Cann. "Perovskite phase formation and ferroelectric properties of the PNN-PZN-PZT ternary system" *Journal of Materials Research* **18**: 2882 (2003)

2. **N. Vittayakorn**, G. Rujijanagul, T. Tunkasiri, X. Tan and D. P. Cann, "Influence of processing conditions on the phase transition and ferroelectric properties of $Pb(Zn_{1/3}Nb_{2/3})O_3$-$Pb(Zr_{1/2}Ti_{1/2})O_3$ ceramics," *Materials Science and Engineering: B.,* **108**:258-265(2004)

3. David P. Cann, Ross Martin, Christi Taylor, **N. Vittayakorn** "Conductivity anomaly in $CuInGaO_4$ and $CuIn2Ga_2O_7$ ceramics" *Materials letters*, **58** : 2141-2151(2004)

4. **N. Vittayakorn**, G. Rujijanagul, X, Tan, M. A. Marquardt, and D. P. Cann, "The morphotropic phase boundary and dielectric properties of $xPb(Zr_{1/2}Ti_{1/2})O_3 - (1-x)Pb(Ni_{1/3}Nb_{2/3})O_3$ binary solid solution" *Journal of Applied Physics*., **96**(9):5103-5109(2004)

5. David P. Cann, G. Rujijanagul , M. Marquardt, X. Tan and **N. Vittayakorn** "Influence of Processing Conditions on the Morphotropic Phase Boundaries and Ferroelectric Properties of $Pb(Zn_{1/3}Nb_{2/3})O_3-Pb(Ni_{1/3}Nb_{2/3})O_3-Pb(Zr_{1/2}Ti_{1/2})O_3$ System" *Proceeding of the 14th IEEE International Symposium on Applications of Ferroelectrics (ISAF-'04),* August 2004, p. 274-277 (2004).

6. **N. Vittayakorn**, G. Rujijanagul, X, Tan, and D. P. Cann "Dielectric properties and morphotropic phase boundaries in the $xPb(Zn_{1/3}Nb_{2/3})O_3 -(1-x)Pb(Zr_{1/2}Ti_{1/2})O_3$ pseudo-binary system" *submitted to the Journal of electroceramics*.

7. **N. Vittayakorn,**G. Rujijanagul, X, Tan, and D. P. Cann **"**Piezoelectric properties of $(1-x)Pb(Zr_{1/2}Ti_{1/2})O_3-xPb(Zn_{1/3}Nb_{2/3})O_3$ ceramics prepared by the columbite-(wolframite) precursor method" *Current Applied Physics* (in press)